Stem cell homeostasis in the root of *Arabidopsis* involves cell type specific complex formation of key transcription factors

Vivien I. Strotmann[1], Monica L. García-Gómez[3,4,5], Yvonne Stahl[1,2,‡*]

Affiliation

[1]Institute for Developmental Genetics, Heinrich-Heine University, Universitätsstraße 1, 40225 Düsseldorf, Germany

[2]Cluster of Excellence on Plant Sciences (CEPLAS), Heinrich-Heine University, Universitätsstraße 1, 40225 Düsseldorf, Germany

[3]Theoretical Biology and Bioinformatics (IBB), Utrecht University, Padualaan 8, 3584 CS Utrecht, The Netherlands

[4]Experimental and Computational Plant Development (IEB), Utrecht University, Padualaan 8, 3584 CS Utrecht, The Netherlands

[5]CropXR Institute, The Netherlands

*Correspondence should be addressed to Y.S. (email: y.stahl@bio.uni-frankfurt.de)

‡Present address: Institute for Molecular Biosciences, Goethe-Universität, Max-von-Laue Str. 9, 60438 Frankfurt am Main, Germany

Key words: mathematical modelling; root stem cell niche; FRET-FLIM; transcription factor complexes; PLTs; WOX5; BRAVO

Date of submission: 26/04/2024

Number of Figures: 8

Total word count: 7603

1

Abstract

In *Arabidopsis thaliana*, the stem cell niche (SCN) within the root apical meristem (RAM) is maintained by an intricate regulatory network that ensures optimal growth and high developmental plasticity. Yet, many aspects of this regulatory network of stem cell quiescence and replenishment are still not fully understood. Here, we investigate the interplay of the key transcription factors (TFs) BRASSINOSTEROID AT VASCULAR AND ORGANIZING CENTRE (BRAVO), PLETHORA 3 (PLT3) and WUSCHEL-RELATED HOMEOBOX 5 (WOX5) involved in SCN maintenance. Phenotypical analysis of mutants involving these TFs uncover their combinatorial regulation of cell fates and divisions in the SCN. Moreover, interaction studies employing fluorescence resonance energy transfer fluorescence lifetime imaging microscopy (FRET-FLIM) in combination with novel analysis methods, allowed us to quantify protein-protein interaction (PPI) affinities as well as higher-order complex formation of these TFs. We integrated our experimental results into a computational model, suggesting that cell type specific profiles of protein complexes and characteristic complex formation, that is also dependent on prion-like domains in PLT3, contribute to the intricate regulation of the SCN. We propose that these unique protein complex 'signatures' could serve as a read-out for cell specificity thereby adding another layer to the sophisticated regulatory network that balances stem cell maintenance and replenishment in the *Arabidopsis* root.

Introduction

51   As sessile organisms, plants must cope with environmental challenges and adapt
52   their growth and development accordingly, as they cannot escape adverse
53   conditions. The root system of higher plants plays a pivotal role for the plant's
54   fitness, as it provides anchorage to the soil and access to water and nutrients. To
55   ensure high developmental plasticity, plants maintain a reservoir of stem cells that
56   reside in the root apical meristem (RAM) at the tip of the root. In *Arabidopsis thaliana*
57   (*A. thaliana*), the center of the RAM harbours a group of slowly dividing, pluripotent
58   stem cells termed the quiescent centre (QC). The QC exerts two key functions: first
59   it produces the surrounding tissue-specific stem cells, also referred to as initials,
60   which by asymmetric cell divisions give rise to different cell types from the outside
61   to the inside: epidermis/lateral root cap, cortex, endodermis, pericycle and stele, as
62   well as the columella at the root tip (Fig. 1 G). Second, the QC serves as signalling
63   hub to maintain the surrounding stem cells in a non-cell autonomous manner (Dolan
64   *et al.*, 1993; van den Berg *et al.*, 1997; Benfey and Scheres, 2000). The balance
65   between QC quiescence and stem cell replenishment has to be maintained
66   throughout the entire life cycle of a plant and therefore requires fine-tuned
67   regulation, necessitating phytohormones, receptors and their ligands as well as
68   several key transcription factors (TFs) (García-Gómez *et al.*, 2021; Strotmann and
69   Stahl, 2021).

70   The homeodomain TF WUSCHEL-RELATED HOMEOBOX 5 (WOX5) was shown
71   to act as a key regulator for stem cell maintenance in the root (Sarkar *et al.*, 2007).
72   By repressing *CYCLIN D3;3* (*CYCD3;3*) and *CYCLIN D1;1* (*CYCD1;1*), WOX5
73   inhibits periclinal cell divisions in the QC (Forzani *et al.*, 2014). Furthermore, WOX5
74   preserves the undifferentiated status of the columella stem cells (CSCs) by
75   repressing *CYCLING DOF FACTOR 4* (*CDF4*), which involves the recruitment of
76   TOPLESS (TPL) and HISTONE DEACETYLASE 19 (HDA19) (Pi *et al.*, 2015).
77   Recent findings suggest that to control the balance between maintaining the stem
78   cell fate of CSCs and their differentiation, WOX5 also interacts with the auxin-
79   dependent APETALA2-type TF PLETHORA 3 (PLT3) (Burkart *et al.*, 2022). The *PLT*
80   gene family comprises six members that are described as master regulators of root
81   development (Aida *et al.*, 2004; Galinha *et al.*, 2007; Mähönen *et al.*, 2014). While
82   PLT5 and 7 are mainly involved in lateral root development (Hofhuis *et al.*, 2013; Du
83   and Scheres, 2017), PLT1-4 are expressed in the main root forming instructive

84　protein gradients that are necessary for correct QC positioning and cell fate

85　decisions (Aida *et al.*, 2004; Galinha *et al.*, 2007; Mähönen *et al.*, 2014).

86　Interestingly, loss of PLT3 or WOX5 function, as observed in *plt3-1* and *wox5-1*

87　mutants, causes an increase of QC divisions (Sarkar *et al.*, 2007; Pi *et al.*, 2015;

88　Burkart *et al.*, 2022). This phenotype is even more severe in the *plt3 wox5* double

89　mutant indicating that PLT3 and WOX5 act in parallel pathways to control stem cell

90　maintenance in the root (Burkart *et al.*, 2022).

91　In the past decade the brassinosteroids (BRs), a class of phytohormones, were

92　described to play an important role in the regulation of the root stem cell niche (SCN)

93　maintenance (González-García *et al.*, 2011). In the *Arabidopsis* RAM, BRs act via

94　the R2R3-MYB TF BRASSINOSTEROIDS AT VASCULAR AND ORGANIZING

95　CENTRE (BRAVO) which inhibits QC divisions and is negatively regulated by the

96　BR-dependent repressor complex formed by BRI1-EMS-SUPPRESSOR 1 (BES1)

97　and TPL on transcript and protein level (Vilarrasa-Blasi *et al.*, 2014; Espinosa-Ruiz

98　*et al.*, 2017). Recently, the ability of BRAVO to control formative QC divisions was

99　linked to WOX5 (Betegón-Putze *et al.*, 2021), as *bravo-2* mutants, like *wox5-1*

100　mutants, show an increased frequency of QC divisions (Sarkar *et al.*, 2007; Pi *et al.*,

101　2015; Betegón-Putze *et al.*, 2021; Burkart *et al.*, 2022).

102　In addition to the described genetic interactions, one-on-one protein-protein

103　interactions (PPIs) have been reported for WOX5 and PLT3 as well as for BRAVO

104　and WOX5 (Betegón-Putze *et al.*, 2021; Burkart *et al.*, 2022). However, It is still

105　unknown whether these TFs can also form higher order complexes. Additionally, it

106　remains elusive how these genetic and physical interactions could possibly

107　influence the regulation of stem cell maintenance. To unravel the underlying

108　interplay of key TFs in the root SCN, we used an integrative experimental and

109　computational approach to analyze the protein complex formation between WOX5,

110　PLT3 and BRAVO in the cells of the root SCN. Here, we show that cell type specific

111　profiles of protein complexes are formed and align their occurrence with

112　phenotypical SCN defects of the respective mutants. Moreover, by the deletion of

113　specific interaction sites, we could demonstrate that heterodimerization contributes

114　to maintaining stem cells in the root. Altogether, our results suggest that these

115　unique protein complex 'signatures' convey cell type specificity and could explain

116　the different roles played by BRAVO, PLT3 and WOX5 in root SCN maintenance.

4

Results

BRAVO, PLT3 and WOX5 exhibit cell type specific differences in protein abundance in the root SCN

First, we analysed the absolute and relative abundance of BRAVO, PLT3 and WOX5 protein levels in the different cell types found in the SCN of the *Arabidopsis* root, focusing on the stele initials (SIs), QC, CSCs and columella cells (CCs) (Fig. 1 G), by measuring the fluorescence intensity of mVenus (mV) in nuclei of the previously described *pPLT3:PLT3-mV* and *pWOX5:WOX5-mV* translational reporters in *Col-0* WT background (Burkart *et al.*, 2022). Additionally, we generated a stable transgenic *Arabidopsis* line expressing *pBRAVO:BRAVO-mV* also in the *Col-0* WT background. We used the same microscopy settings for these quantifications to ensure that the detected protein levels are comparable. Consistent with previous findings, BRAVO protein levels are highest in the SIs and gradually decrease towards the CCs (Fig. 1 A, B) (Vilarrasa-Blasi *et al.*, 2014). PLT3 levels are similar in SIs, QC and CSCs, but notably lower in the CCs (Fig. 1 C, D). WOX5 protein levels peak in the QC, decrease in the adjacent SIs and CSCs and are almost completely absent in CCs (Fig. 1 E, F).

We summarized our findings in a protein abundance profile for each individual cell type displaying relative protein levels of BRAVO, PLT3 and WOX5. The protein levels are normalized to the overall maximum intensity, which was found for BRAVO in SIs (Fig. 1 H). Accordingly, We found that BRAVO is the most abundant protein in the SIs, followed by PLT3 and WOX5 in descending order. Conversely, in the QC, we observe a contrasting pattern, marked by WOX5 as the most abundant protein, followed by PLT3 and BRAVO. PLT3 emerges as the predominant protein in the adjacent CSCs, accompanied by low levels of WOX5 and BRAVO protein. In differentiated CCs, WOX5 and BRAVO are almost absent and only low levels of PLT3 can be found. Interestingly, while all of these regulators are expressed in several root SCN cells, our observations reveal quantitative differences in protein abundance that can be combined into a cell type specific 'fingerprint'. This provides a comprehensive snapshot of the unique protein levels within each cellular context, which could act as an instructive output of cell type specification (Fig. 1 H).

BRAVO, PLT3 and WOX5 jointly control CSC fate and QC divisions

Several studies have highlighted the inhibitory effect of BRAVO, PLT3 and WOX5 on QC divisions and CSC differentiation in the *Arabidopsis* root (Aida *et al.*, 2004; Galinha *et al.*, 2007; Vilarrasa-Blasi *et al.*, 2014; Mähönen *et al.*, 2014; Forzani *et al.*, 2014; Pi *et al.*, 2015). While all three proteins have been demonstrated to be present in the QC and CSCs, a combinatory effect on QC division and CSC fate has only been demonstrated for WOX5 and PLT3 (Burkart *et al.*, 2022) as well as for WOX5 and BRAVO (Betegón-Putze *et al.*, 2021). Notably, such interplay has not been observed for BRAVO and PLT3, nor for the simultaneous involvement of all three proteins.

To address this, we have performed SCN stainings, that combines 5-ethynyl-2'-deoxyuridine (EdU) and modified pseudo Schiff base propidium iodide (mPS-PI) stainings (Burkart *et al.*, 2022), in several single and multiple mutants. This allowed us to analyse the differentiation status of the distal meristem, as well as the number of QC divisions that occurred within the last 24 h within the same root. To quantify CSC layers, the number of cell layers that lack starch granules distally to the QC were counted. In *Col-0* WT, 68 % of the roots show one CSC layer, whereas only 2 % of the roots lack the starch-free CSC layer and 30 % show two CSC layers, most likely because they have recently divided (Fig. 2 A, B, J, Fig. S1 A). In *bravo-2* and *plt3-1* single mutants, the number of roots showing no CSC layer increases to 11 % and 12 %, respectively (Fig. 2 C, D, J, Fig. S1 B, C). Interestingly, the number of roots displaying no starch-free CSC layer increased to 37 % in *bravo plt3* double mutants (Fig. 2 F, J, Fig. S1 F). This additive effect indicates that PLT3 and BRAVO act in parallel pathways to control CSC differentiation. In 53 % of the *wox5-1* mutant roots, the starch-free CSC layer is missing (Fig. 2 E, J, Fig. S1 D), further emphasizing the importance of WOX5 for CSC fate (Sarkar *et al.*, 2007; Pi *et al.*, 2015; Burkart *et al.*, 2022). Additionally, the *bravo wox5* and the *plt3 wox5* double mutants show an even higher percentage of roots lacking the starch-free CSC, 90 % and 74 % respectively, compared to the single mutants and the *bravo plt3* double mutants (Fig. 2 G, H, J, Fig. S1 E, G). On the other hand, the *bravo plt3 wox5* triple mutant, with 85 % of the roots having a differentiated CSC layer, resembles the *bravo wox5* and *plt3 wox5* double mutants (Fig. 2 I, J, Fig. S1 H). These results suggest that BRAVO, PLT3 and WOX5 jointly control CSC fate.

182 Additionally, the quantification of QC divisions was performed by counting the
183 number of EdU-stained nuclei within an optical transversal section through the RAM
184 as described in (Burkart *et al.*, 2022). QC cells were identified by their relative
185 position within the RAM, directly below the vascular initials and surrounded by CEIs
186 in a circular arrangement (Fig. 2 K). In the WT, 57 % of the roots do not show any
187 QC cell divisions, and 35 % show one QC cell division (Fig. 2 L, T, Fig. S1 A). In 6 %
188 and 2 % of the analysed roots, two and three QC divisions could be observed,
189 respectively, so that in total 43 % of the analysed roots showed EdU-stained QC
190 cells. In *bravo-2* and *plt3-1* single mutants, the number of roots showing at least one
191 EdU-stained QC cell increased to 78 % and 73 %, respectively (Fig. 2 M, N, T, Fig.
192 S1 B, C). This phenotype is even more severe in *wox5-1* mutants, where at least
193 one EdU-stained QC cell could be observed in 86 % of the roots (Fig. 2 O, T, Fig.
194 S1 D). Like the above-described additive effects of CSC differentiation in the double
195 and triple mutants, the number of roots showing at least one QC cell division
196 increases to 100 % and 98 % in the *bravo wox5* and *plt3 wox5* double mutants,
197 respectively (Fig. 2 P-R, T, Fig. S1 E-G). Additionally, the double mutants show a
198 strongly increased frequency of four divided QC cells in comparison to the
199 respective single mutants: 7 % in the *bravo plt3* double mutant, 36 % in the *bravo*
200 *wox5* double mutant and 30 % in the *plt3 wox5* double mutant in comparison to 3 %,
201 0 % and 11 % in the *bravo-2*, *plt3-1* and *wox5-1* single mutants, respectively. A
202 further increase in EdU-stained QC cells can be observed in the *bravo plt3 wox5*
203 triple mutant where 44 % of the roots display a completely divided QC (Fig. 2 S, T,
204 Fig. S1 H). These observations indicate that BRAVO, PLT3 and WOX5 jointly control
205 QC divisions, which may also involve other factors, e. g. SHORT-ROOT (SHR) and
206 SCARECROW (SCR) (Cruz-Ramírez *et al.*, 2013; Long *et al.*, 2017; Clark *et al.*,
207 2020).

208 Furthermore, we also examined if the QC exhibits extra periclinal cell divisions,
209 which in *Col-0* WT occurs only in 4 % of the roots (Fig. S1 I, K). This phenotype
210 manifests in 85 % of *bravo-2* mutants (Fig. S1 J, K). Additional periclinal cell
211 divisions can also be observed in 43 % of *plt3-1* single mutants and in 62 % *wox5-
212 1* single mutants (Fig. S1 K). In contrast to the number of EdU-stained QC cells, the
213 frequency of periclinal cell divisions are relatively similar in the double or triple
214 mutants, with 77 %, 84 %, 79 % and 85 % of the roots showing additional periclinal
215 cell divisions of the QC cells in the *bravo plt3*, *bravo wox5*, *plt3 wox5* and *bravo plt3*

7

216   *wox5* mutants, respectively (Fig. S1 K). This effect has already been described for

217   *wox5-1* and *bravo-2* single mutants in comparison to the *bravo wox5* double mutant

218   in earlier studies (Betegón-Putze *et al.*, 2021).

219   Taken together, our findings suggest a combinatory effect of BRAVO, PLT3, and

220   WOX5 on QC division frequency and CSC fate decision.

221

222   **BRAVO, PLT3 and WOX5 can form a trimeric complex**

223   In addition to the observed overlapping yet cell type specific protein levels and the

224   genetic interplay of BRAVO, PLT3 and WOX5, recent reports also provide evidence

225   for one-on-one PPIs of BRAVO and WOX5, as well as for PLT3 and WOX5

226   (Betegón-Putze *et al.*, 2021; Burkart *et al.*, 2022). These findings raised the question

227   if also BRAVO and PLT3 could interact. To address this, we first performed

228   fluorescence resonance energy transfer fluorescence lifetime imaging microscopy

229   (FRET-FLIM) measurements in transiently expressing *Nicotiana benthamiana* (*N.*

230   *benthamiana*) abaxial epidermal leaf cells using BRAVO-mV as donor molecule

231   under control of a β-estradiol inducible promoter as described earlier (Burkart *et al.*,

232   2022). Results of FRET-FLIM measurements are often displayed as the average

233   amplitude-weighted lifetime which is a mixture of differentially decaying components

234   and is calculated by summing each component's lifetime weighted by its respective

235   amplitude. In case of FRET, the fluorescence lifetime decreases and serves as a

236   measure for PPI. This reduction of lifetime results either from a large number of

237   molecules that undergo FRET indicating a high affinity of the two proteins of interest

238   (POIs) or a highly efficient energy transfer which demonstrates high proximity of the

239   POIs and/or favourable fluorophore dipole orientation (Fig. 3. A, B). The use of a

240   novel analysis method allowed us to distinguish between these two scenarios,

241   providing deeper insights into protein affinities, hereafter referred to as 'binding',

242   between BRAVO, PLT3 and WOX5 (Maika *et al.*, 2023).

243   The reference sample BRAVO-mV (donor-only control) shows an average binding

244   of 2.3 ± 7.4 % (Fig. 3 C) and the negative control composed of BRAVO-mV co-

245   expressed with mCherry-NLS shows a binding of 8.8 ± 4.3 % (Fig. 3 C). A binding

246   of below 10 % is interpreted as no interaction (Maika *et al.*, 2023), cohering with the

247   reference and negative control samples. Upon co-expression of BRAVO-mV with

248   PLT3-mCh, the binding increases to 28.0 ± 11.7 % (Fig. 3 C). To compare this

249   observation with already confirmed interactions of BRAVO with WOX5 (Betegón-

8

250   Putze *et al.*, 2021), as well as with BES1 or TPL (Vilarrasa-Blasi *et al.*, 2014), we

251   co-expressed BRAVO-mV with WOX5-mCh or TPL-mCh, which results in binding

252   values of 22.4 ± 14.1 % and 26.7 ± 9.8 %, respectively (Fig. 3 C). Interaction of

253   BRAVO with BES1 was tested by co-expression of BRAVO-mV with BES1D-mCh,

254   which was shown to mimic the dephosphorylated and thereby active form of BES1

255   and yielded an average binding of 27.4 ± 11.9 %. This suggests similar affinities of

256   BRAVO towards PLT3, BES1 and TPL, but a lower affinity towards WOX5 (Fig. 3

257   C).

258   These findings together with previously described interactions of WOX5 with PLT3,

259   TPL or BES1, as well as BES1 and TPL, prompted us to investigate, whether these

260   TFs can also form higher-order complexes (Vilarrasa-Blasi *et al.*, 2014; Espinosa-

261   Ruiz *et al.*, 2017; Betegón-Putze *et al.*, 2021; Burkart *et al.*, 2022). To address this,

262   we used a combination of bimolecular fluorescence complementation (BiFC) and

263   FRET (Fig. 4 A, B) (Kwaaitaal *et al.*, 2010; Maika *et al.*, 2023). Here, the donor

264   fluorophore is split into two fragments: the N-terminal part of mVenus (mV(N)) and

265   the C-terminal part (mV(C)). The interaction of WOX5 and PLT3, which has been

266   described earlier (Burkart *et al.*, 2022), has been shown to have a high affinity

267   (Supplemental table S13). This is why we have chosen to tag WOX5 and PLT3 with

268   mV(N) and mV(C), respectively. In this scenario, the interaction of WOX5 and PLT3

269   leads to the reconstruction of mV and restores its fluorescence, enabling us to

270   perform FRET-FLIM when co-expressing another acceptor-labelled protein. The

271   'donor only' reference sample WOX5-mV(N) PLT3-mV(C) yields an average binding

272   of 1.6 ± 14.1 %, and the negative control WOX5-mV(N) PLT3-mV(C) with mCherry-

273   NLS shows an average binding of 2.9 ± 5.0 % (Fig. 4 C). Upon co-expression of

274   BES1D-mCh or TPL-mCh, the binding significantly increases to 18.7 ± 8.0 % and

275   23.3 ± 8.3 %, respectively (Fig. 4 C). Notably, in the presence of BRAVO-mCh, the

276   average binding strongly increases to 36.3 ± 10.7 % (Fig. 4 C). Thus, the

277   heterodimer of WOX5 and PLT3 shows higher affinity to BRAVO, which could

278   suggest an increased probability and stability of the trimeric complex composed of

279   WOX5, PLT3 and BRAVO compared to WOX5, PLT3 and BES1D, or TPL.

280   To gain further insights into the potential of trimeric complex formation, we

281   conducted additional FRET-FLIM measurements in *N. benthamiana* with rearranged

282   fluorescent tags. Here, the donor fluorophore is shared between BRAVO and PLT3,

283   namely BRAVO-mV(N) and PLT3-mV(C), which also showed high affinity (Fig. 3).

284   The 'donor only' reference sample BRAVO-mV(N) PLT3-mV(C) exhibits an average

285   binding of 2.2 ± 3.6 % (Fig. S2). The negative control composed of BRAVO-mV(N)

286   PLT3-mV(C) and mCherry-NLS shows a similar average binding of 3.2 ± 3.1 % (Fig.

287   S2). Surprisingly, co-expression of BES1D-mCh yields an average binding of only

288   10.2 ± 5.9 % (Fig. S2), indicating that a trimeric complex composed of BRAVO, PLT3

289   and BES1D is unlikely to form. Contrary, the co-expression of TPL-mCh or WOX5-

290   mCh leads to a significantly increased average binding of 21.1 ± 8.3 % and

291   29.8 ± 10.6 %, respectively (Fig. S2). This again suggests that a trimeric complex

292   formed by BRAVO, PLT3 and WOX5 is more stable and occurs with a higher

293   probability. Taken together, these findings reveal the formation of several

294   combinations of protein multimers with different probabilities of occurrence as

295   judged by their binding capacities. Here, the complex composed of BRAVO, PLT3

296   and WOX5 seems to be the most frequent and stable.

297

298   **Modelling reveals cell type specific TF complex compositions**

299   Our results reveal distinct, cell type specific patterns of protein abundance for

300   BRAVO, PLT3 and WOX5 in the root SCN (Fig. 1) along with the formation of diverse

301   heterodimers with varying binding affinities as well as higher-order complexes in *N.*

302   *benthamiana* (Fig. 3, Fig. 4, Fig. S2). The protein complexes formed in the cells of

303   the root SCN are ultimately a result of the cell type specific protein levels and the

304   binding affinities between the proteins. This raises the question whether

305   dimerization and complex formation in the context of the root apex also display cell

306   type specificity, and how this is influenced by the protein levels in each cell of the

307   SCN (Fig. 1). For example, BRAVO protein levels in the QC are notably lower

308   compared to PLT3 or WOX5 (Fig. 1 H), yet its consequence on protein complex

309   formation remains undetermined. While the FRET-FLIM approach could in theory

310   be used to investigate the formation of dimer- and oligomerization in *Arabidopsis*

311   root cells, previous efforts to assess the interaction of PLT3 and WOX5 under the

312   control of their endogenous promoter in roots have been challenging due to limited

313   protein abundance and, consequently, low photon counts (Burkart *et al.*, 2022). This

314   is a limitation difficult to overcome without altering the endogenous protein levels.

315   Therefore, as an alternative to identify potential TF specificity and cell type specific

316   complexes in the root SCN, we use a two-step mathematical modelling approach

317   that combines the endogenous protein abundances (Fig.1) with the binding

10

318   probabilities for one-on-one PPIs and trimeric protein complexes (Fig. 3, Fig. 4, Fig.
319   S2).

320   First, we performed a parameter analysis to predict the relative association and
321   dissociation rates to form the WOX5-PLT3, BRAVO-PLT3, BRAVO-WOX5
322   heterodimers, and the WOX5-PLT3-BRAVO trimeric complex. For the trimeric
323   complex, we evaluate its formation via WOX5-PLT3 and BRAVO-PLT3 as donors
324   (Fig. 4, Fig. S2). We start our simulations with equal levels of both donor and
325   acceptor as initial condition, to mimic the conditions in the *N. benthamiana*
326   experiments. Then, we simulate the protein complex formation using association
327   and dissociation rates from a wide range of possible parameter values, until a steady
328   state is reached. For each parameter combination tested, we evaluated if the
329   proportion of protein in complex in steady state corresponds to the value from the
330   respective relative binding affinity determined with our experiments. Repeating this
331   parameter estimation for each of the protein complexes under study, allows us to
332   identify several parameter combinations capable of producing protein complexes in
333   line with FRET-FLIM experimental data (Fig. S3, Fig. S4). The predicted parameter
334   combination for protein complexes with a high binding affinity (i.e. WOX5-PLT3) fall
335   in the space where association rates are higher than the dissociation rates (Fig. S3),
336   in contrast to lower binding affinity complexes (i.e. BRAVO-WOX5). These
337   determined parameters allow us to describe our binding experimental data in a
338   computational model.

339   Next, we simulated the protein complexes formed by BRAVO, WOX5 and PLT3 in
340   each of the cells of the root SCN. For this, we use as initial condition the values from
341   the relative fluorescence intensities we quantified for BRAVO, PLT3 and WOX5 in
342   the SI, QC, CSC, and CC (Fig. 1 H), and the association/dissociation rates per
343   complex from our parameter analysis. Therefore, the cell type specific profiles of
344   protein complexes predicted by modelling are the emergent result of how much
345   protein is available in each cell type and the binding affinities between specific
346   protein pairs and complexes (Fig. 5). We summarized these results in a radar chart
347   where the level of each protein complex is arranged in a different radial axis and
348   displayed free protein levels that remain after complex formation separately as bar
349   plots (Fig. 5 A, B). Furthermore, we combined these results in a heat map (Fig. 5
350   C). Additionally, we performed several controls that assume different combinations
351   of experimental data, both binding affinities and cell type specific protein

352 abundances, and varying ratios of association and dissociation (Fig. S5, Material
353 and Methods). Interestingly, results comparable to our model were only observed in
354 control 2, assuming higher association and dissociation rates, which indicates
355 higher association also in our experimental data.

356 Our simulation reveals that SIs are characterized by high levels of BRAVO-PLT3
357 protein complex (Fig. 5 A, C). The QC cells are predicted to be enriched in the
358 WOX5-PLT3 complexes, followed closely by the CSC. Such enrichment could be
359 related to the previously described function of the WOX5-PLT3 complex in QC
360 divisions and CSC maintenance (Burkart *et al.*, 2022). However, predictions of the
361 trimeric complex WOX5-PLT3-BRAVO displays only intermediate levels in both the
362 SI and the QC. Finally, the CCs are predicted to have negligible levels of all protein
363 complexes studied, consistent with the very low BRAVO, PLT3, and WOX5 protein
364 levels present in these cells according to our quantification (Fig. 1). Notably, these
365 protein complex 'signatures' are strikingly different in each of the simulated cells and
366 the resulting polygons are unique for each cell type (Fig. 5 A), which might be related
367 to their specific function.

368 Curiously, the levels of free protein also show cell type specific patterns, that allow
369 to further distinguish between SIs, QC and CSCs (Fig. 5 B, C). SIs are enriched in
370 free BRAVO, while the QC shows high levels of free WOX5. Both, CSCs and CCs,
371 exhibit high levels of PLT3. It is interesting to consider that these free proteins could
372 participate in both, binding other proteins not considered here, and/or intercellular
373 movement, assuming an increased mobility if the protein is not in complexes (Fig. 5
374 B, C). For instance, the levels of free WOX5 in the QC cells could constitute a pool
375 of free protein available for intercellular mobility towards the neighbouring CSCs as
376 previously described (Pi *et al.*, 2015). In summary, these results support the
377 hypothesis that complex formation, especially heterodimerization, occurs in a cell
378 type specific context.

379

Prion-like domains of PLT3 serve as conserved interaction hub

381 After we have found evidence for the formation of TF complexes with cell type
382 dependent variations, we asked whether these complexes are important for root
383 SCN maintenance. To address this, we aimed to destabilize the interaction of these
384 TFs by mutating their specific interaction sites and observe if this altered protein can
385 still rescue the phenotypical defects in the SCN. First, we explored the literature to

386   identify potential interaction sites of BRAVO, PLT3 and WOX5. Previous studies
387   have shown that prion-like domains (PrDs) in PLT3 mediate the interaction with
388   WOX5 (Burkart *et al.*, 2022). PrDs are intrinsically disordered regions (IDRs) and
389   serve not only as mediators of multivalent interactions, but have also been
390   demonstrated to be involved in chromatin opening (Levy *et al.*, 2002) and phase
391   separation (Jung *et al.*, 2020). Given the presence of PrDs also in PLT1, PLT2 and
392   PLT4, albeit in lower numbers (Burkart *et al.*, 2022), we hypothesized that these
393   regions function as conserved interaction sites. Thus, we performed FRET-FLIM
394   measurements to investigate how the deletion of PLT3 PrDs, termed PLT3ΔPrD,
395   affects its interaction with BRAVO. The 'donor only' reference control BRAVO-mV
396   yields an average binding of 1.7 ± 4.6 %, which increases to 3.9 ± 2.4 % in the
397   presence of mCherry-NLS serving as negative control (Fig. 6). Upon co-expression
398   of BRAVO-mV with PLT3-mCh the binding significantly increases to 22.8 ± 10.5 %
399   (Fig. 6). However, BRAVO-mV co-expressed with PLT3ΔPrD-mCh yields an
400   average binding of only 11.7 ± 9.6 %, suggesting that the deletion of the PrDs
401   significantly reduces the interaction of PLT3 with BRAVO.
402   To further support our hypothesis that the PrDs in PLTs act as conserved interaction
403   site, we investigated whether PLT3 also interacts with BES1 and TPL, which were
404   shown before for to interact with BRAVO and WOX5 (Vilarrasa-Blasi *et al.*, 2014; Pi
405   *et al.*, 2015; Betegón-Putze *et al.*, 2021) and if this interaction can also be altered
406   by the deletion of PLT3 PrDs. To address this, we conducted FRET-FLIM in the
407   presence of an acceptor-labelled PLT3 or PLT3ΔPrD. For the donor only reference
408   control measurements BES1D-mV, an average binding of 0.0 ± 6.3 % could be
409   observed which increases to 16.9 ± 8.1 % in the presence of PLT3-mCh indicating
410   PPI (Fig. S6 A). However, co-expression of BES1D-mV with PLT3ΔPrD-mCh shows
411   a reduced binding of 8.4 ± 4.8 % which is not significantly different from the negative
412   control BES1D-mV with mCherry-NLS exhibiting an average binding of 4.9 ± 6.5 %
413   (Fig. S6 A). The reference control TPL-mV exhibits an average binding of 0.6 ± 5.5
414   %, increasing to 6.4 ± 2.4 % when co-expressed with the negative control mCherry-
415   NLS (Fig. S6 B). Upon co-expression of TPL-mV with PLT3-mCh, the average
416   binding significantly increases to 13.5 ± 4.3 %, suggesting a moderate interaction of
417   TPL with PLT3 (Fig. S6 B). Similar to BES1, the interaction of TPL and PLT3 is also
418   abolished by the deletion of PrDs, demonstrated by a significantly decreased
419   average binding of 8.99 ± 5.26 % for TPL-mV with PLT3ΔPrD-mCh (Fig. S6). In

13

420 summary, these findings support the idea that the PrDs of PLT3 serve as a

421 conserved interaction site for numerous TFs present in the root SCN.

422

Redistribution of TF complexes alters regulation of QC divisions

424 Next, we aimed to analyse the functional relevance of the eliminated or reduced

425 interaction of PLT3 with other TFs present in the *Arabidopsis* root by deleting its

426 PrDs. To address this, we created two transgenic *Arabidopsis* lines, using either full-

427 length PLT3 or PLT3ΔPrD C-terminally tagged with mTurquoise2 (mT2) in

428 combination with the dexamethasone (DEX) inducible glucocorticoid receptor (GR)

429 in the *plt3-1* mutant background. Using the *WOX5* promoter allowed us to

430 specifically investigate how the loss of PLT3 PrD influences QC maintenance. These

431 lines were named *pWOX5:GR-PLT3-mT2* (*pWOX5:iPLT3)* and *pWOX5:GR-*

432 *PLT3ΔPrD-mT2* (*pWOX5:iPLT3ΔPrD)*. Finally, we performed a SCN staining and

433 investigated if the QC exhibits additional periclinal cell divisions after inducing the

434 plants by DEX treatment or in the presence of dimethyl sulfoxide (DMSO), which

435 serves as a control (Fig. 7 A-I).

436 Under control conditions, only 27 % of *Col-0* WT roots show additional periclinal cell

437 divisions in the QC, which does not change significantly in the presence of DEX (Fig.

438 7 A, E, I). In agreement with previous observations (Burkart *et al.*, 2022), *plt3-1*

439 single mutant roots show additional periclinal cell divisions in the QC of 73 % under

440 control conditions and 87 % after induction with DEX (Fig. 7 B, F, I). In *pWOX5:iPLT3*

441 and *pWOX5:iPLT3ΔPrD* transgenic lines, 83 % and 94 % of the roots exhibit a

442 periclinal cell division in the QC under control conditions, respectively, which is even

443 higher than the *plt3-1* single mutant (Fig. 7 C, D, I). However, in the presence of

444 DEX, only 67 % of the roots expressing *pWOX5:iPLT3* show this phenotype,

445 indicating that full-length PLT3 in the QC partially restores the *plt3-1* periclinal cell

446 division phenotype (Fig. 7 G, I). Contrary, the observed overproliferated phenotype

447 that we see under control conditions in *pWOX5:iPLT3ΔPrD* mutant roots, is

448 unaffected in the presence of DEX, indicating that the PrDs of PLT3 are necessary

449 to inhibit additional periclinal QC divisions and thereby contribute to PLT3 function

450 in root SCN maintenance (Fig. 7 H, I).

451 After observing the reduced affinity of PLT3ΔPrD for BRAVO and WOX5, and that it

452 was unable to rescue SCN defects in *plt3-1* single mutants, we decided to use our

453 computational model to predict immediate changes in the protein complex

14

454   'signatures' in the root SCN that may have contributed to this failed rescue. Thus,

455   we simulated the protein complex formation in the SI, QC, CSC, and CC as

456   described before but set the association rate of PLT3ΔPrD-WOX5 to zero (Burkart

457   *et al.*, 2022) and use the binding affinity we have determined experimentally for

458   PLT3ΔPrD-BRAVO (Fig. 6 and S6). This leads to a dramatic shift in the protein

459   complex 'signatures' of the root SCN cells (Fig. 7 J-L). The elimination of WOX5-

460   PLT3 dimer formation causes a redistribution of PLT3 and WOX5 to the other protein

461   complexes and an increase of free PLT3 and WOX5 protein levels in the SI and the

462   QC cells, as well as higher levels of free PLT3 in the CSC (Fig. 7 J, K). While the

463   BRAVO-PLT3 complex can still be formed, it is noticeably reduced in the SI, QC and

464   CSC cells. Furthermore, the BRAVO-WOX5 complex levels increase in the SI and

465   QC cells. Surprisingly, the profile of the trimeric complex shows only minor

466   disruptions in the modelled cells. Therefore, even if the WOX5-PLT3 protein

467   complex cannot be formed due to the removal of PLT3 PrDs, the trimeric complex

468   can still be formed by the association of WOX5 with the BRAVO-PLT3 protein

469   complex. Altogether, our PLT3ΔPrD simulation provides insights into the alterations

470   on cell type specific protein levels that could be causative for defects observed

471   experimentally in the root SCN.

Discussion

In the past decades, our understanding of stem cell function and maintenance in the root of *Arabidopsis* has witnessed significant advances. Various aspects, including hormonal, developmental, as well as stress-related mechanisms have been discovered (Nolan *et al.*, 2020; García-Gómez *et al.*, 2021; Ubogoeva *et al.*, 2021; Strotmann and Stahl, 2021). However, the underlying intricate network of molecular factors, still remains largely enigmatic. In this study, we aimed to unravel a new aspect of the regulatory network that controls root SCN maintenance, related to protein complex formation.

By utilizing a distinct SCN staining technique (Burkart *et al.*, 2022), we assessed phenotypical defects in the architecture of the *Arabidopsis* root SCN of several single and multiple mutants (Fig. 2). We observed an increased CSC differentiation and an elevated periclinal QC division frequency in the SCN of *plt3-1* mutants (Burkart *et al.*, 2022). The observed phenotypes agree with previous observations, and their relatively moderate phenotypic manifestation can be attributed to the substantial redundancy within the PLT TF family (Galinha *et al.*, 2007; Burkart *et al.*, 2022). Moreover, these observations are consistent with a uniform PLT3 protein abundance in SIs, QC and CSCs (Fig. 1). Compared to *plt3-1* single mutants, we could observe a stronger effect for QC division frequency in *bravo-2* single mutants but a similar mild phenotype for CSC differentiation. Again, these results are supported by the observed protein levels: Although BRAVO is most abundant in SIs, it can also be found in the QC, whereas it is notably reduced in CSCs. *wox5-1* single mutants show a severely defective root SCN, as demonstrated by the loss of CSCs and greatly increased periclinal QC divisions, as described before (Sarkar *et al.*, 2007; Cruz-Ramírez *et al.*, 2013; Pi *et al.*, 2015; Betegón-Putze *et al.*, 2021; Burkart *et al.*, 2022). Similar to PLT3 and BRAVO, these phenotypes correlate with high WOX5 protein levels in the QC and less protein in the CSC where WOX5 was shown to move to (Pi *et al.*, 2015; Berckmans *et al.*, 2020).

In the *bravo plt3*, *bravo wox5*, and *plt3 wox5* double mutants, we observed an increase in both QC division frequency and CSC differentiation, that were consistently higher than the respective single mutants. For PLT3 and WOX5 such additive effects have been described before and were hypothesized to show that they act in parallel pathways to maintain the integrity of the root SCN (Burkart *et al.*, 2022). However, previous findings suggest that BRAVO and WOX5 act in the same

16

506 pathway to control CSC fate and QC divisions based on quantifications of additional

507 periclinal cell divisions (Betegón-Putze *et al.*, 2021). We could observe similar

508 effects when analysing periclinal cell divisions in the QC but using a novel SCN

509 staining technique, we observed additive effects for QC division alterations in the

510 *bravo wox5* double mutant compared to the respective single mutants (Fig. 2, Fig.

511 S1). Our findings suggest the presence of an additional pathway that involves

512 BRAVO and PLT3. Moreover, this indicates that these TFs could act in three

513 independent constellations to regulate SCN maintenance. However, in the *bravo*

514 *plt3 wox5* triple mutant, an additional additive effect could only be observed for QC

515 divisions but not for CSC differentiation. A potential interpretation of these results is

516 that none of these TFs is involved in an additional pathway to control CSC

517 differentiation. However, they may partially contribute to other pathways that inhibit

518 QC divisions. Additional functions in other independent pathways have already been

519 described for WOX5 in the SHR-SCR regulatory network (Cruz-Ramírez *et al.*,

520 2013; Zhai *et al.*, 2020; Clark *et al.*, 2020). Additionally, TEOSINTE-

521 BRANCHED/CYCLOIDEA/PCNA 20 (TCP20) was found to mediate the interaction

522 of PLT3 and SCR, to specify the QC and establish the root SCN (Shimotohno *et al.*,

523 2018). If and to what extent these molecular factors genetically interact with other

524 TFs in the SCN, will be an interesting perspective for future investigations.

525 In addition to the identified genetic interplay of BRAVO, PLT3 and WOX5 regarding

526 root SCN maintenance, we were able to evaluate their physical interaction (Fig. 3,

527 Supplementary Table S13). While interactions of PLT3 and WOX5 as well as

528 BRAVO and WOX5, have been described before (Betegón-Putze *et al.*, 2021;

529 Burkart *et al.*, 2022), evidence for an interaction of PLT3 and BRAVO was still

530 missing. Our results reveal for the first time PPI between BRAVO and PLT3 as well

531 as between PLT3 and BES1 and TPL (Fig. 3, Fig. S6). Together with previously

532 described, independent one-on-one interactions, these findings support the

533 hypothesis of three parallel pathways that control CSC differentiation and QC

534 divisions in parallel. Furthermore, the observed variations of stability and probability

535 of occurrence as indicated by a special analysis tool (Orthaus *et al.*, 2009; Maika *et*

536 *al.*, 2023), could indicate a specific mechanism that facilitates the interaction of two

537 POIs in a highly dynamic microenvironment, where the number of proteins is

538 generally high, such as in the QC. (Fig. 1).

17

539   Next, the combination of BiFC and FRET allowed us to investigate the formation of

540   higher-order complexes (Fig. 4, Fig. S2). Like in the one-on-one interaction studies,

541   we found differences in protein affinities of the complexes under investigation. Here,

542   the trimeric complex formed by WOX5-PLT3-BRAVO appeared to be the most

543   abundant and stable. The heterodimerization of transcriptional regulators increases

544   binding specificity and affinity and allows the combination of different internal as well

545   as external signal inputs into gene regulation (Strader *et al.*, 2022). This idea is

546   reinforced when considering that both the auxin-regulated WOX5 and BR-

547   dependent BRAVO have been demonstrated to control the same cell cycle-related

548   genes (*CYCD1;1, CYCD3;3*) (Forzani *et al.*, 2014; Vilarrasa-Blasi *et al.*, 2014). So

549   far, cell cycle-related downstream targets of PLT3 remain unknown. Further

550   investigations are necessary to uncover potentially common downstream targets of

551   BRAVO, PLT3 and WOX5.

552   To elaborate on differences in protein abundance and complex formation in cells of

553   the root SCN, we used a computational modelling approach. This strategy allowed

554   us to describe cell type specific protein complex profiles in WT roots (Fig. 5). Here,

555   the combination of high levels of the BRAVO-PLT3 heterodimer and high levels of

556   free BRAVO appears to be characteristic for stele initials. Interestingly, BRAVO

557   protein abundance not only decreased when moving distally from the SIs, but also

558   in proximal direction (Fig. 1). However, alterations of SCN defects in *bravo-2* single

559   mutants had only been evaluated for CSC differentiation and QC division. New

560   phenotypical analyses are necessary to determine whether SIs and their

561   descendants are also affected upon loss of BRAVO function.

562   Our simulations of protein 'signatures' revealed that both, QC as well as CSC, are

563   enriched in the WOX5-PLT3 heterodimer, which aligns with their previously

564   described impact on QC divisions and CSC differentiation (Burkart *et al.*, 2022).

565   However, the protein 'signatures' of QC and CSC could be distinguished when free

566   protein levels were considered. In the QC, our model predicted high protein levels

567   of free WOX5, while CSCs were predicted to possess higher levels of PLT3. Several

568   studies highlighted the elevated abundance of WOX5 in the QC, which could be

569   either linked to interactions with other proteins not analysed here or its non-cell

570   autonomous function in the adjacent initials, although its necessity as mobile

571   stemness factor is still under debate (Pi *et al.*, 2015; Berckmans *et al.*, 2020). The

572   predicted high levels of PLT3 protein in CSCs might be linked to nuclear body (NB)

18

573 formation of PLT3, which was linked to its PrDs and is concentration dependent and

574 may involve PLT3 homomerization. This mechanism could facilitate the recruitment

575 of the WOX5-PLT3 heterodimer into these pre-formed NBs, as demonstrated

576 previously (Burkart *et al.*, 2022).

577 In CCs, the absence of BRAVO and WOX5 hinders complex formation, resulting in

578 high levels of free PLT3. However, compared to CSC PLT3 levels are notably lower

579 accompanied with loss of NBs formation. This implies that a specific protein

580 concentration is required to initially trigger NB formation highlighting the difference

581 between differentiated CCs and the stem cell fate determination process in CSCs.

582 Based on our results, we created a final model that summarizes the described

583 protein 'signatures' (Fig. 8). Here, SIs are characterized by high levels of free

584 BRAVO protein and the heterodimer BRAVO-PLT3. QC cells and CSCs possess

585 elevated levels of the WOX5-PLT3 heterodimer, which is accompanied by high

586 levels of free WOX5 in the QC and high levels of free PLT3 in CSC. In CCs, complex

587 formation is hindered by negligible levels of BRAVO and WOX5, resulting in elevated

588 levels of free PLT3. All together our findings imply the formation of dimers that

589 together with differences of free protein levels convey cell type specificity in the root.

590 In the future, it should be addressed how the predicted protein complex 'signatures'

591 drive changes in gene expression, including *BRAVO*, *PLT3*, and *WOX5*, but also

592 other target genes, and how this relates to QC division and CSC number alterations

593 in single and multiple mutants. As a next step, the model could also consider the

594 complex gene regulatory networks in the root SCN (Cruz-Ramírez *et al.*, 2012;

595 García-Gómez *et al.*, 2017; Pardal and Heidstra, 2021), the role of cell-cell mobility

596 of free protein (Mähönen *et al.*, 2014; Pi *et al.*, 2015; García-Gómez *et al.*, 2020;

597 Betegón-Putze *et al.*, 2021), the presence of membrane-less compartments to

598 account for the localization of WOX5-PLT3 in nuclear bodies in the CSC (Burkart *et*

599 *al.*, 2022) and other key regulatory processes involved. The integration of

600 experimental and computational approaches holds promise to uncover these

601 complex mechanisms underlying root SCN maintenance.

602 To investigate the impact of heterodimer- and oligomerization on root SCN

603 maintenance, we aimed to identify potential interaction sites in the BRAVO, PLT3 or

604 WOX5 amino acid sequence. Previous studies revealed that PrDs found in PLT3 act

605 as mediator of its interaction with WOX5 (Burkart *et al.*, 2022). PrDs are also present

606 in PLT1,2 and 4 which is also accompanied by NB formation. However, PLT3

607　harbours the highest number of PrDs, which correlates with stronger NB formation

608　compared to PLT1, 2 and 4. Here, we demonstrated that loss of PrDs also negatively

609　influences PLT3 interaction with BRAVO, BES1 and TPL (Fig. 6, Fig. S6). These

610　findings suggest that PrDs act as a multivalent interaction hub, which could also

611　indicate a conserved function among other PLTs.

612　In a rescue experiment, we could demonstrate that the PrDs of PLT3 affect its ability

613　to inhibit periclinal QC divisions by demonstrating that PLT3ΔPrD, expressed in the

614　QC, is unable to rescue the *plt3-1* periclinal QC division phenotype (Fig. 7). This

615　indicates that correct dimer- and oligomerization is necessary for proper QC

616　maintenance. We integrated our findings of diminished interactions of PLT3ΔPrD

617　with BRAVO and WOX5 to our model and found a severe shift of protein complex

618　'signatures', especially for the WOX5-PLT3 dimer in the QC and CSCs. This further

619　strengthens our hypothesis that the protein complexes form instructive protein

620　signatures important for cell fate decisions in the *Arabidopsis* root SCN.

621　Interestingly, full-length PLT3 under control of the *WOX5* promoter only partially

622　rescues the *plt3-1* periclinal QC division phenotype. This emphasizes that functional

623　PLT3 is also necessary to locally maintain CSC fate and repress differentiation as

624　the QC divides to replenish lost CSCs (Cruz-Ramírez *et al.*, 2013). Furthermore,

625　this could indicate a specific function for PLT3 in the CSC fate, as the presence of

626　other PLTs was not able to fully compensate for the loss of PLT3. Previous findings

627　in yeast suggest that differences in IDRs mediate specificity of transcription factors

628　that share the same DNA-binding motif (Brodsky *et al.*, 2020). This is often observed

629　among TFs that belong to the same family. If a similar mechanism also exists in

630　plants, this could suggest that PLT3 function in CSC fate is specifically linked to its

631　PrDs and that, due to their differentially structured PrDs, the other PLTs cannot

632　compensate for this specific function. Additionally, this could indicate that mobile

633　PLT3 which might move from the QC to CSC is not enough to maintain CSC stem

634　cell character.

635　IDRs or PrDs also play a role in a recently described alternative mechanism of how

636　TF find and locate to their specific DNA target (Staller, 2022). Indeed, the majority

637　of TF found in eukaryotes is mainly composed of IDRs and only a small fraction of

638　the protein sequence is well-characterized (Ward *et al.*, 2004; Wang *et al.*, 2016).

639　According to this theory, IDRs of TFs scan the genome for matching protein clouds

640　which mediate binding of the DNA-binding domain to its specific genomic target site

20

641 (Staller, 2022). TFs possess two main functions: bind other TFs and bind to their

642 specific DNA target to alter gene expression (Strader *et al.*, 2022). Some TFs

643 possess an additional important role; pioneer transcription factors, like LEAFY (Lai

644 *et al.*, 2021; Jin *et al.*, 2021), bind to nucleosome bound DNA, open the target locus,

645 e.g. by displacing H1 linker histones and/or recruiting chromatin remodellers, and

646 make it accessible for other TFs. In plants, the concept of pioneer transcription

647 factors is a newly emerging research field, but studies in animals suggest, that

648 'master regulators' appear to be promising candidates for pioneer transcription

649 factors (as reviewed in Yamaguchi, 2021). The identification of IDRs and/or PrDs,

650 that possess the ability to facilitate multivalent interaction and have been shown to

651 act in chromatin opening (Levy *et al.*, 2002), together with high redundancy within

652 the PLT TF family, their role as master regulators of root formation and the stable

653 protein abundance in the SCN, especially in cells that possess stem cell character,

654 could indicate that also PLTs act as pioneer transcription factors in the root SCN.

655 Interestingly, DNA affinity purification-sequencing (DAP-seq) results found PLT3, as

656 well as PLT7, to be highly enriched in mCG-methylated DNA, providing yet another

657 hint for this theory (O'Malley *et al.*, 2016). Nevertheless, more evidence is necessary

658 to further support the potential function of PLTs as pioneer transcription factor in root

659 SCN maintenance.

660 Overall, our results suggest that BRAVO, PLT3 and WOX5 form cell type specific

661 profiles of protein complexes and that proper complex formation contributes to

662 optimal stem cell maintenance. Furthermore, we propose that these unique protein

663 complex signatures serve as a read-out for cell specificity and could explain the

664 different roles played by BRAVO, PLT3 and WOX5 in the regulation of stem cell

665 homeostasis in the root.

Material and Methods

Plant work

All *Arabidopsis thaliana* lines used in this study were in *Col-0* background and can be found in Appendix Table S5. The *wox5-1* and *plt3-1* single mutants (Galinha *et al.*, 2007) as well as the *bravo-2* single mutant (Vilarrasa-Blasi *et al.*, 2014) and *bravo-2 wox5-1* double mutant (Betegón-Putze *et al.*, 2021) were described before. The *bravo-2 plt3-1* double and *bravo-2 plt3-1 wox5-1* triple mutants were created by crossings. Homozygous F3 plants were verified by PCR using appropriate primers (Appendix Table S2). Transgenic lines were created by the floral dip method (Zhang *et al.*, 2006). The *pPLT3:PLT3-mV* and *pWOX5:WOX5-mV* translational reporters in *Col-0* WT background were described earlier (Burkart *et al.*, 2022). For *pBRAVO:BRAVO-mVenus*, *pWOX5:GR-PLT3-mTurquoise2,* and *pWOX5:GR-PLT3ΔPrD-mTurquoise2* transgenic plants, lines were selected, that possess a single T-DNA insertion, which was tested by observing the segregation on selection marker containing plates. Plants for crossing, genotyping, transformation, floral dip and amplification were grown under long-day conditions (8 h dark, 16 h light) at 21 °C and 60 % humidity. For microscopy, seeds were sterilized with chlorine gas (50 ml 13 % sodium hypochlorite (v/v), 1 ml hydrochloric acid) in a desiccator, mounted in 0.15 % (w/v) agarose and stratified in the dark at 4 °C for minimum two days before sowing on GM agar plates without sucrose (1/2 MS including Gamborg B5 vitamins, 1.2 % plant agar (w/v) and 0.05 % MES hydrate (w/v)). Seedlings for imaging were grown for five to six days under continuous light at 80 µmol m^{-2} s^{-1}, 21 °C and 60 % humidity.

Cloning

Plasmids for the transgenic lines *pBRAVO:BRAVO-mVenus*, *pWOX5:GR-PLT3-mTurquoise2* and *pWOX5:GR-PLT3ΔPrD-mTurquoise2* as well as for transient expression in *N. benthamiana* were generated using the GreenGate cloning method in the pGGZ001 destination vector (Lampropoulos *et al.*, 2013). The region of the *WOX5* promoter, the CDS of WOX5, PLT3 and PLT3ΔPrD CDS as well as WOX5, PLT3 and PLT3ΔPrD constructs for transient expression in *N. benthamiana* were described before (Burkart *et al.*, 2022). The region upstream of the transcriptional start of BRAVO (2,925 bp) (Lee *et al.*, 2006) was assigned as promoter and

22

699 amplified by PCR with appropriate primers containing flanking *Bsa*I restriction sites

700 and matching overlaps for GreenGate cloning. The internal *Bsa*I recognition site in

701 the *BRAVO* promoter region was not removed, but incubation times for restriction

702 digestion and GreenGate reaction were adapted accordingly. After PCR, the

703 promoter sequence was cloned into the GreenGate entry vector pGGA000 using

704 *Bsa*I restriction and ligation. The CDS of BRAVO and TPL were amplified from cDNA

705 derived from extracted RNA by PCR using primers carrying the *Bsa*I recognition site

706 and matching GreenGate overhangs. Next, they were cloned into the GreenGate

707 entry vector pGGC000 via restriction digest and ligation. All entry vectors were

708 confirmed by sequencing. The GreenGate entry vector carrying the β-estradiol

709 inducible promoter cassette was provided by (Denninger *et al.*, 2019). For

710 bimolecular fluorescence complementation, the GreenGate M and N intermediate

711 vectors, each of which carried one expression cassette, were used. The correct

712 assembly of the modules was confirmed by sequencing. All module combinations,

713 constructs as well as primers used for cloning are listed in Appendix Tables S4, S3,

714 and S1, respectively.

715

SCN staining

717 SCN staining was performed according to (Burkart *et al.*, 2022). For CSC layer

718 quantification, optical longitudinal sections of the *Arabidopsis* root were acquired.

719 The cell layer below the QC was scored as differentiated if three or more cells in this

720 layer accumulated starch granules. QC cell divisions were quantified using an

721 optical cross-section of the RAM on a scale of zero to four or more cells. If the QC

722 was duplicated and showed two layers, as often seen for *bravo-2* mutants, only QC

723 divisions in the upper layer were counted.

724 The CSC layer and QC cell division phenotypes were visualized separately in bar

725 plots using Microsoft Excel (Microsoft Office 365, Microsoft Corporation). To assess

726 potential correlations between CSC layers and QC divisions, data were combined

727 into 2D-plots showing QC division on the x-axis and CSC layer on the y-axis using

728 Origin 2021b (OriginLab Corporation).

729

Transient expression in *Nicotiana benthamiana*

731 For transient expression in *N. benthamiana*, the *Agrobacterium* strain

732 GV3101::pMP50 was used that in addition to the plasmid harbouring the desired

23

733   construct, carried the helper plasmid pSOUP needed for GreenGate vectors.

734   *Agrobacteria* were grown overnight in 5 ml dYT medium at 28 °C with shaking. After

735   centrifugation for 10 min at 4,000 rpm and 4 °C, the pellet was resuspended in

736   infiltration medium (5 % sucrose (w/v), 0.01 % $MgSO_4$ (w/v), 0.01 % glucose (w/v)

737   and 450 µM acetosyringone) to an optical density OD_{600} of 0.6 and mixed with an

738   *Agrobacterium* strain carrying the p19 silencing repressor and eventually with a

739   second *Agrobacterium* strain carrying a different construct for co-expression.

740   Subsequently, the cultures were incubated for 1 h at 4 °C. To trigger stomatal

741   opening and thereby allow easy infiltration, *N. benthamiana* plants were sprayed

742   with water and kept under high humidity prior to infiltration. The abaxial side of the

743   leaf was infiltrated using a syringe without a needle. Expression was induced 2-4

744   days after infiltration by spraying a 20 µM β-estradiol solution containing 0.1 %

745   Tween®-20 (v/v) to the abaxial side of the leaf. Depending on the expression level,

746   FLIM measurements were performed 2-16 h after induction.

747

Microscopy

749   Imaging of *Arabidopsis thaliana* roots was performed using an inverted ZEISS

750   LSM780 or LSM880. For cell wall staining, Arabidopsis seedlings were mounted in

751   an aqueous solution of propidium iodide (PI) (10 µM). Fluorophores and fluorescent

752   dyes were excited and detected as follows: PI was excited with 561 nm and detected

753   at 590-670 nm; Alexa Fluor® 488 was excited at 488 and detected at 500-580 nm;

754   mVenus was excited at 514 nm and detected at 520-570 nm and mCherry was

755   excited at 561 nm and detected at 580-680 nm. When mVenus was co-expressed

756   with mCherry, it was excited at 488 nm and detected at 505-555 nm.

757

Intensity measurements of protein levels in *A. thaliana*

759   For analysis of expression levels of different reporters in 6 DAG *Arabidopsis* roots

760   of different genotypes, an inverted LSM880 microscope with constant settings for all

761   reporters was used. The mean fluorescence levels were measured in ImageJ using

762   an oval region of interest (ROI) of the size of one nucleus. One to three nuclei were

763   measured per cell type and root of which the mean was calculated. Data were

764   normalized to mean value of the combination cell type and reporter that yielded the

765   highest intensity. Data result from three technical replicates.

766

24

Induction of GR inducible Arabidopsis lines

For the *plt3-1* rescue experiments, seeds were sown on GM agar plates without sucrose (1/2 MS including Gamborg B5 vitamins, 1.2 % plant agar (w/v) and 0.05 % MES hydrate (w/v)) containing either 0.1 % DMSO (v/v) for control condition or 20 µM DEX (diluted in DMSO) for GR induction. After 5 days, seedlings were transferred to GM agar plates without sucrose containing 7 µg/ml 5-ethynyl-2'-deoxyuridine (EdU) and either 0.1 % DMSO (v/v) or 20 µM DEX (diluted in DMSO) and grown for 24 h. SCN staining, imaging and scoring of QC divisions and CSC layers were performed as described above.

FRET-FLIM measurements

FRET-FLIM measurements were performed in transiently expressing epidermal leaf cells of 3 to 4 weeks old *N. benthamiana* using an inverted ZEISS LSM 780 equipped with additional time-correlated single-photon counting devices (Hydra Harp 400, PicoQuant GmbH) and a pulsed laser diode. mVenus was chosen as donor and excited at 485 nm with 1 µW laser power at the objective (40 x C-Apochromat/1.2 Corr W27, ZEISS) and a frequency of 32 MHz and detected using two τ-SPAD single photon counting detectors in perpendicular and parallel orientation. Photons were collected over 40 frames at 256x256 pixels per frame, a pixel dwell time of 12.6 µs and a digital zoom of 8. Prior to image acquisition, a calibration routine was performed. To test system functionality, fluorescence correlation spectroscopy (FCS) measurements of deionized water and Rhodamine110 were acquired. Additionally, monitoring the decay of erythrosine B in saturated potassium iodide served as instrument response function (IRF) to correct the fitting for system specific time shift between laser pulse and data acquisition. First, fluorescence decays of the donor-only control were analysed using the 'Grouped FLIM' analysis tool to determine the average fluorescence lifetime using a mono- or biexponential fitting model (SymPhoTime, PicoQuant GmbH). Next, to extract information about protein affinities and proximities, the 'Grouped LT FRET Image' tool was utilized for a monoexponentially decaying donor and the 'One Pattern Analysis (OPA)' tool was used for samples with a biexponentially decaying donor (SymPhoTime, PicoQuant GmbH). These tools allow separate analyses of the amplitude and fluorescence lifetime of the FRET fraction of each sample. Consequently, the amplitude of the FRET component serves as a measure for the

801   number of molecules undergoing FRET, termed binding or protein affinity, whereas

802   the difference of the fluorescence lifetime of the FRET component compared to the

803   lifetime of the donor-only fraction is used to calculate the FRET efficiency which

804   serves as a measure for protein proximity and orientation (Maika *et al.*, 2023). For

805   samples where molecules do not undergo FRET e.g., the donor-only and negative

806   control, binding values mostly varied between - 10 and 10 % and corresponding

807   FRET efficiencies mostly accumulated at 10 or 80 %, which was defined during the

808   fitting process (Maika *et al.*, 2023).

809

810   **Statistical tests**

811   Data were tested for normal distribution by Shapiro test (α = 0.05) followed by a

812   Levene's test for equality of variances (α = 0.05). Since some data did not show

813   normal distribution or equality of variances or both, all data sets were tested with a

814   non-parametric Kruskal-Wallis ANOVA with *post-hoc* Dunn's test (α = 0.05).

815   Statistical testing was performed using R.

816

817   **Protein complex modelling**

818   To estimate the relative association and dissociation rates for each of the dimeric

819   and trimeric complexes studied here, we used the following ordinary differential

820   equations:

821

822   (1)

823
$$\frac{dDA}{dt} = a \cdot A \cdot D - d \cdot DA$$

824   (2)

825
$$\frac{dA}{dt} = d \cdot DA - a \cdot A \cdot D$$

826   (3)

827
$$\frac{dD}{dt} = d \cdot DA - a \cdot A \cdot D$$

828

829   where *DA* is the protein complex formed by donor protein *D* and acceptor protein *A*.

830   Using these equations, we simulated that the amount of protein complex, *DA*, is

831   determined by the product of the association rate (*a*), the concentrations of donor,

832   *D*, and acceptor, *A*, proteins, and how much it dissociates given a certain

26

833 dissociation rate (*d*). To explain the relative binding affinity values determined

834 experimentally for each dimeric and trimeric protein complex, we assessed

835 association and dissociation rates involved in the protein complex formation from a

836 wide range (0 – 0.5 arbitrary units, step 0.001), and simulated the protein complex

837 *AB* formation until a steady state was reached. We deemed a particular combination

838 of association and dissociation rates successful if they produce a value of *AB* at

839 steady state in line with the relative binding affinity rates. In this way, we were able

840 to predict relative binding rates for the dimeric and trimeric protein complexes

841 studied here.

842   Next, we simulated the protein complex formation in the cells of the root SCN

843 using the following ordinary differential equations to describe the formation of each

844 dimeric and trimeric complex:

845

846 (4)

847 $$\frac{dWOX5}{dt} = d_{BRAVOWOX5} \cdot BRAVOWOX5 + d_{WOX5PLT3} \cdot WOX5PLT3 + d_{WOX5PLT3BRAVO2}$$

848 $$\cdot WOX5PLT3BRAVO - WOX5 \cdot (a_{BRAVOWOX5} \cdot BRAVO + a_{WOX5PLT3}$$

849 $$\cdot PLT3 + a_{WOX5PLT3BRAVO2} \cdot BRAVOPLT3)$$

850 (5)

851 $$\frac{dBRAVO}{dt} = d_{BRAVOWOX5} \cdot BRAVOWOX5 + d_{BRAVOPLT3} \cdot BRAVOPLT3$$

852 $$+ d_{WOX5PLT3BRAVO1} \cdot WOX5PLT3BRAVO - BRAVO \cdot (a_{BRAVOWOX5}$$

853 $$\cdot WOX5 + a_{BRAVOPLT3} \cdot PLT3 + a_{WOX5PLT3BRAVO1} \cdot WOX5PLT3)$$

854 (6)

855 $$\frac{dPLT3}{dt} = d_{BRAVOPLT3} \cdot BRAVOPLT3 + d_{WOX5PLT3} \cdot WOX5PLT3 - PLT3 \cdot (a_{BRAVOPLT3}$$

856 $$\cdot BRAVO + a_{WOX5PLT3} \cdot WOX5)$$

857 (7)

858 $$\frac{dWOX5PLT3}{dt} = a_{WOX5PLT3} \cdot WOX5 \cdot PLT3 - d_{WOX5PLT3} \cdot WOX5PLT3$$

859 $$- a_{WOX5PLT3BRAVO1} \cdot WOX5PLT3 \cdot BRAVO + d_{WOX5PLT3BRAVO1}$$

860 $$\cdot WOX5PLT3BRAVO$$

861 (8)

862 $$\frac{dBRAVOPLT3}{dt}$$

863 $$= a_{BRAVOPLT3} \cdot BRAVO \cdot PLT3 - d_{BRAVOPLT3} \cdot BRAVOPLT3$$

864 $$- a_{WOX5PLT3BRAVO2} \cdot WOX5PLT3 \cdot BRAVO + d_{WOX5PLT3BRAVO2}$$

865 $$\cdot WOX5PLT3BRAVO$$

866 (9)

867 $$\frac{dBRAVOWOX5}{dt} = a_{BRAVOWOX5} \cdot BRAVO \cdot WOX5 - d_{BRAVOWOX5} \cdot BRAVOWOX5$$

868 (10)

869 $$\frac{dWOX5PLT3BRAVO}{dt}$$

870 $$= a_{WOX5PLT3BRAVO1} \cdot WOX5PLT3 \cdot BRAVO + a_{WOX5PLT3BRAVO2}$$

871 $$\cdot BRAVOPLT3 \cdot WOX5$$

872 $$- WOX5PLT3BRAVO \cdot (d_{WOX5PLT3BRAVO1} + d_{WOX5PLT3BRAVO2})$$

873

874 Notice the trimeric complex can be formed either by the binding of BRAVO to WOX5-

875 PLT3, or WOX5 to BRAVO-PLT3. Then, we modelled the protein complexes formed

876 in the cells of the root SCN using equations 4-10 and the relative protein levels of

877 WOX5, BRAVO and PLT3 determined for SI, QC, CSC, and CC cells as initial

878 condition. As several sets of binding rates were predicted per complex, for these

879 simulations we used one selected at random. Notably, the specific parameters used

880 for the results we present here do not change the protein complex signatures

881 predicted by the model (Fig. S4).

882 To evaluate the effect in our model of both, the cell type specific protein levels as

883 well as differential binding affinities are necessary for our model, we performed

884 different control simulations. On the one hand, we tested the effect of equal

885 association/dissociation rates ($a = d = 0.1$), higher association than dissociation

886 rate ($a = 0.1, d = 0.05$), and lower association than dissociation ($a = 0.05, d = 0.1$)

887 for all protein complexes using our experimental protein level quantification in the

888 SI, QC, CSC and CC displayed as Control 1-3, respectively (Fig. S5). On the other

889 hand, we consider an alternative scenario where all proteins have the same

890 abundance levels, while the association/dissociation rates are based on our binding

891 data (Control 4, Fig. S5). Finally, we consider the scenarios where the control

892 conditions   meet   pairwise: Control   5   is   a   combination   of   equal

893 association/dissociation rate together with the assumption of equal protein

894   abundances among cell types and proteins. In Control 6, the equality of protein
895   levels is combined with higher association than dissociation rates. Finally, Control 7
896   combines lower association that dissociation rates with equal protein abundances
897   (Fig. S5). Notably only control 2, which uses experimentally determined protein
898   abundances together with a higher association than dissociation rate, produced
899   results comparable to our model. Thus, leading to the conclusion that also in our
900   experimental data, association rates must be higher than dissociations rates.
901   Moreover, this indicates a key role of the protein levels in each cell in the resulting
902   protein complex and free protein signatures. In all other cases, we could observe
903   strikingly different protein complex 'signatures' to those we described with the model
904   that uses our experimental data, indicating that our findings result from the
905   combination of experimentally determined specific protein levels and binding
906   affinities.

907   The code for the computational model generated in this study was implemented in
908   R, and will be available at the Garcia Group webpage in the server of the Theoretical
909   Biology and Bioinformatics Group (https://bioinformatics.bio.uu.nl/monica/Cell type-
910   specific-complex-formation-of-key-transcription-factors-in-the-root-SCN)   and   in
911   GitHub (https://github.com/moneralee/Cell type-specific-complex-formation-of-key-
912   transcription-factors-in-the-root-SCN) upon publication.

913

914

915

Acknowledgements

938

939 Author contributions

940 Y.S. conceived the project. Y.S. and V.I.S. designed, analyzed and interpreted the
941 data. V.I.S. carried out all experiments. M.L.G.G. formulated and performed
942 mathematical modelling. The manuscript was written by V.S. and M.L.G.G. and was
943 revised by Y.S. All authors commented and approved the manuscript.
944

945 Declaration of competing interests

946 The authors declare no competing interests.
947

948

949 This manuscript has not been accepted or published elsewhere.
950

References

Aida M, Beis D, Heidstra R *et al.* 2004. The PLETHORA genes mediate patterning of the Arabidopsis root stem cell niche. *Cell* **119,** 109–120.

Benfey PN, Scheres B. 2000. Root development. *Current biology CB* **10,** R813-5.

Berckmans B, Kirschner G, Gerlitz N, Stadler R, Simon R. 2020. CLE40 Signaling Regulates Root Stem Cell Fate. *Plant physiology* **182,** 1776–1792.

Betegón-Putze I, Mercadal J, Bosch N *et al.* 2021. Precise transcriptional control of cellular quiescence by BRAVO/WOX5 complex in Arabidopsis roots. *Molecular systems biology* **17,** e9864.

Brodsky S, Jana T, Mittelman K *et al.* 2020. Intrinsically Disordered Regions Direct Transcription Factor In Vivo Binding Specificity. *Molecular cell* **79,** 459-471.e4.

Burkart RC, Strotmann VI, Kirschner GK *et al.* 2022. PLETHORA-WOX5 interaction and subnuclear localization control Arabidopsis root stem cell maintenance. *EMBO reports* **23,** e54105.

Clark NM, Fisher AP, Berckmans B *et al.* 2020. Protein complex stoichiometry and expression dynamics of transcription factors modulate stem cell division. *Proceedings of the National Academy of Sciences of the United States of America* **117,** 15332–15342.

Cruz-Ramírez A, Díaz-Triviño S, Blilou I *et al.* 2012. A bistable circuit involving SCARECROW-RETINOBLASTOMA integrates cues to inform asymmetric stem cell division. *Cell* **150,** 1002–1015.

Cruz-Ramírez A, Díaz-Triviño S, Wachsman G *et al.* 2013. A SCARECROW-RETINOBLASTOMA protein network controls protective quiescence in the Arabidopsis root stem cell organizer. *PLoS biology* **11,** e1001724.

Denninger P, Reichelt A, Schmidt VAF *et al.* 2019. Distinct RopGEFs Successively Drive Polarization and Outgrowth of Root Hairs. *Current biology CB* **29,** 1854-1865.e5.

Dolan L, Janmaat K, Willemsen V *et al.* 1993. Cellular organisation of the Arabidopsis thaliana root. *Development (Cambridge, England)* **119,** 71–84.

Du Y, Scheres B. 2017. PLETHORA transcription factors orchestrate de novo organ patterning during Arabidopsis lateral root outgrowth. *Proceedings of the National Academy of Sciences of the United States of America* **114,** 11709–11714.

983 **Espinosa-Ruiz A, Martínez C, Lucas M** de *et al.* 2017. TOPLESS mediates
984 brassinosteroid control of shoot boundaries and root meristem development in
985 Arabidopsis thaliana. *Development (Cambridge, England)* **144,** 1619–1628.

986 **Forzani C, Aichinger E, Sornay E** *et al.* 2014. WOX5 suppresses CYCLIN D
987 activity to establish quiescence at the center of the root stem cell niche. *Current*
988 *biology CB* **24,** 1939–1944.

989 **Galinha C, Hofhuis H, Luijten M** *et al.* 2007. PLETHORA proteins as dose-
990 dependent master regulators of Arabidopsis root development. *Nature* **449,**
991 1053–1057.

992 **García-Gómez ML, Azpeitia E, Álvarez-Buylla ER.** 2017. A dynamic genetic-
993 hormonal regulatory network model explains multiple cellular behaviors of the
994 root apical meristem of Arabidopsis thaliana. *PLoS computational biology* **13,**
995 e1005488.

996 **García-Gómez ML, Garay-Arroyo A, García-Ponce B, La Sánchez MdP,**
997 **Álvarez-Buylla ER.** 2021. Hormonal Regulation of Stem Cell Proliferation at the
998 Arabidopsis thaliana Root Stem Cell Niche. *Frontiers in plant science* **12,**
999 628491.

1000 **García-Gómez ML, Ornelas-Ayala D, Garay-Arroyo A, García-Ponce B, La**
1001 **Sánchez MdP, Álvarez-Buylla ER.** 2020. A system-level mechanistic
1002 explanation for asymmetric stem cell fates: Arabidopsis thaliana root niche as a
1003 study system. *Scientific reports* **10,** 3525.

1004 **González-García M-P, Vilarrasa-Blasi J, Zhiponova M** *et al.* 2011.
1005 Brassinosteroids control meristem size by promoting cell cycle progression in
1006 Arabidopsis roots. *Development (Cambridge, England)* **138,** 849–859.

1007 **Hofhuis H, Laskowski M, Du Y** *et al.* 2013. Phyllotaxis and rhizotaxis in
1008 Arabidopsis are modified by three PLETHORA transcription factors. *Current*
1009 *biology CB* **23,** 956–962.

1010 **Jin R, Klasfeld S, Zhu Y** *et al.* 2021. LEAFY is a pioneer transcription factor and
1011 licenses cell reprogramming to floral fate. *Nature communications* **12,** 626.

1012 **Jung J-H, Barbosa AD, Hutin S** *et al.* 2020. A prion-like domain in ELF3 functions
1013 as a thermosensor in Arabidopsis. *Nature* **585,** 256–260.

1014 **Kwaaitaal M, Keinath NF, Pajonk S, Biskup C, Panstruga R.** 2010. Combined
1015 bimolecular fluorescence complementation and Forster resonance energy

1016   transfer reveals ternary SNARE complex formation in living plant cells. *Plant*
1017   *physiology* **152,** 1135–1147.

1018   **Lai X, Blanc-Mathieu R, GrandVuillemin L *et al.*** 2021. The LEAFY floral regulator
1019   displays pioneer transcription factor properties. *Molecular plant* **14,** 829–837.

1020   **Lampropoulos A, Sutikovic Z, Wenzl C, Maegele I, Lohmann JU, Forner J.**
1021   2013. GreenGate---a novel, versatile, and efficient cloning system for plant
1022   transgenesis. *PloS one* **8,** e83043.

1023   **Lee J-Y, Colinas J, Wang JY, Mace D, Ohler U, Benfey PN.** 2006. Transcriptional
1024   and posttranscriptional regulation of transcription factor expression in
1025   Arabidopsis roots. *Proceedings of the National Academy of Sciences of the*
1026   *United States of America* **103,** 6055–6060.

1027   **Levy YY, Mesnage S, Mylne JS, Gendall AR, Dean C.** 2002. Multiple roles of
1028   Arabidopsis VRN1 in vernalization and flowering time control. *Science (New*
1029   *York, N.Y.)* **297,** 243–246.

1030   **Long Y, Stahl Y, Weidtkamp-Peters S *et al.*** 2017. In vivo FRET-FLIM reveals cell
1031   type-specific protein interactions in Arabidopsis roots. *Nature* **548,** 97–102.

1032   **Mähönen AP, Tusscher K** ten, **Siligato R *et al.*** 2014. PLETHORA gradient
1033   formation mechanism separates auxin responses. *Nature* **515,** 125–129.

1034   **Maika JE, Krämer B, Strotmann VI *et al.*** 2023. One pattern analysis (OPA) for the
1035   quantitative determination of protein interactions in plant cells. *Plant methods* **19,**
1036   73.

1037   **Nolan TM, Vukašinović N, Liu D, Russinova E, Yin Y.** 2020. Brassinosteroids:
1038   Multidimensional Regulators of Plant Growth, Development, and Stress
1039   Responses. *The Plant cell* **32,** 295–318.

1040   **O'Malley RC, Huang S-SC, Song L *et al.*** 2016. Cistrome and Epicistrome Features
1041   Shape the Regulatory DNA Landscape. *Cell* **165,** 1280–1292.

1042   **Orthaus S, Buschmann V, Bäter A, Fore S, König M, Erdmann R.** 2009.
1043   Quantitative in vivo imaging of molecular distances using FLIM-FRET.

1044   **Pardal R, Heidstra R.** 2021. Root stem cell niche networks: it's complexed! Insights
1045   from Arabidopsis. *Journal of experimental botany* **72,** 6727–6738.

1046   **Pi L, Aichinger E, van der Graaff E *et al.*** 2015. Organizer-Derived WOX5 Signal
1047   Maintains Root Columella Stem Cells through Chromatin-Mediated Repression
1048   of CDF4 Expression. *Developmental cell* **33,** 576–588.

1049 **Sarkar AK, Luijten M, Miyashima S *et al.*** 2007. Conserved factors regulate
1050 signalling in Arabidopsis thaliana shoot and root stem cell organizers. *Nature*
1051 **446,** 811–814.

1052 **Shimotohno A, Heidstra R, Blilou I, Scheres B.** 2018. Root stem cell niche
1053 organizer specification by molecular convergence of PLETHORA and
1054 SCARECROW transcription factor modules. *Genes & development* **32,** 1085–
1055 1100.

1056 **Staller MV.** 2022. Transcription factors perform a 2-step search of the nucleus.
1057 *Genetics* **222**.

1058 **Strader L, Weijers D, Wagner D.** 2022. Plant transcription factors - being in the
1059 right place with the right company. *Current opinion in plant biology* **65,** 102136.

1060 **Strotmann VI, Stahl Y.** 2021. At the root of quiescence: function and regulation of
1061 the quiescent center. *Journal of experimental botany* **72,** 6716–6726.

1062 **Strotmann VI, Stahl Y.** 2022. Visualization of in vivo protein-protein interactions in
1063 plants. *Journal of experimental botany* **73,** 3866–3880.

1064 **Ubogoeva EV, Zemlyanskaya EV, Xu J, Mironova V.** 2021. Mechanisms of stress
1065 response in the root stem cell niche. *Journal of experimental botany* **72,** 6746–
1066 6754.

1067 **van den Berg C, Willemsen V, Hendriks G, Weisbeek P, Scheres B.** 1997. Short-
1068 range control of cell differentiation in the Arabidopsis root meristem. *Nature* **390,**
1069 287–289.

1070 **Vilarrasa-Blasi J, González-García M-P, Frigola D *et al.*** 2014. Regulation of plant
1071 stem cell quiescence by a brassinosteroid signaling module. *Developmental cell*
1072 **30,** 36–47.

1073 **Wang C, Uversky VN, Kurgan L.** 2016. Disordered nucleiome: Abundance of
1074 intrinsic disorder in the DNA- and RNA-binding proteins in 1121 species from
1075 Eukaryota, Bacteria and Archaea. *Proteomics* **16,** 1486–1498.

1076 **Ward JJ, Sodhi JS, McGuffin LJ, Buxton BF, Jones DT.** 2004. Prediction and
1077 functional analysis of native disorder in proteins from the three kingdoms of life.
1078 *Journal of molecular biology* **337,** 635–645.

1079 **Yamaguchi N.** 2021. LEAFY, a Pioneer Transcription Factor in Plants: A Mini-
1080 Review. *Frontiers in plant science* **12,** 701406.

1081 **Zhai H, Zhang X, You Y, Lin L, Zhou W, Li C.** 2020. SEUSS integrates
1082 transcriptional and epigenetic control of root stem cell organizer specification.
1083 *The EMBO journal* **39,** e105047.
1084 **Zhang X, Henriques R, Lin S-S, Niu Q-W, Chua N-H.** 2006. Agrobacterium-
1085 mediated transformation of Arabidopsis thaliana using the floral dip method.
1086 *Nature protocols* **1,** 641–646.
1087
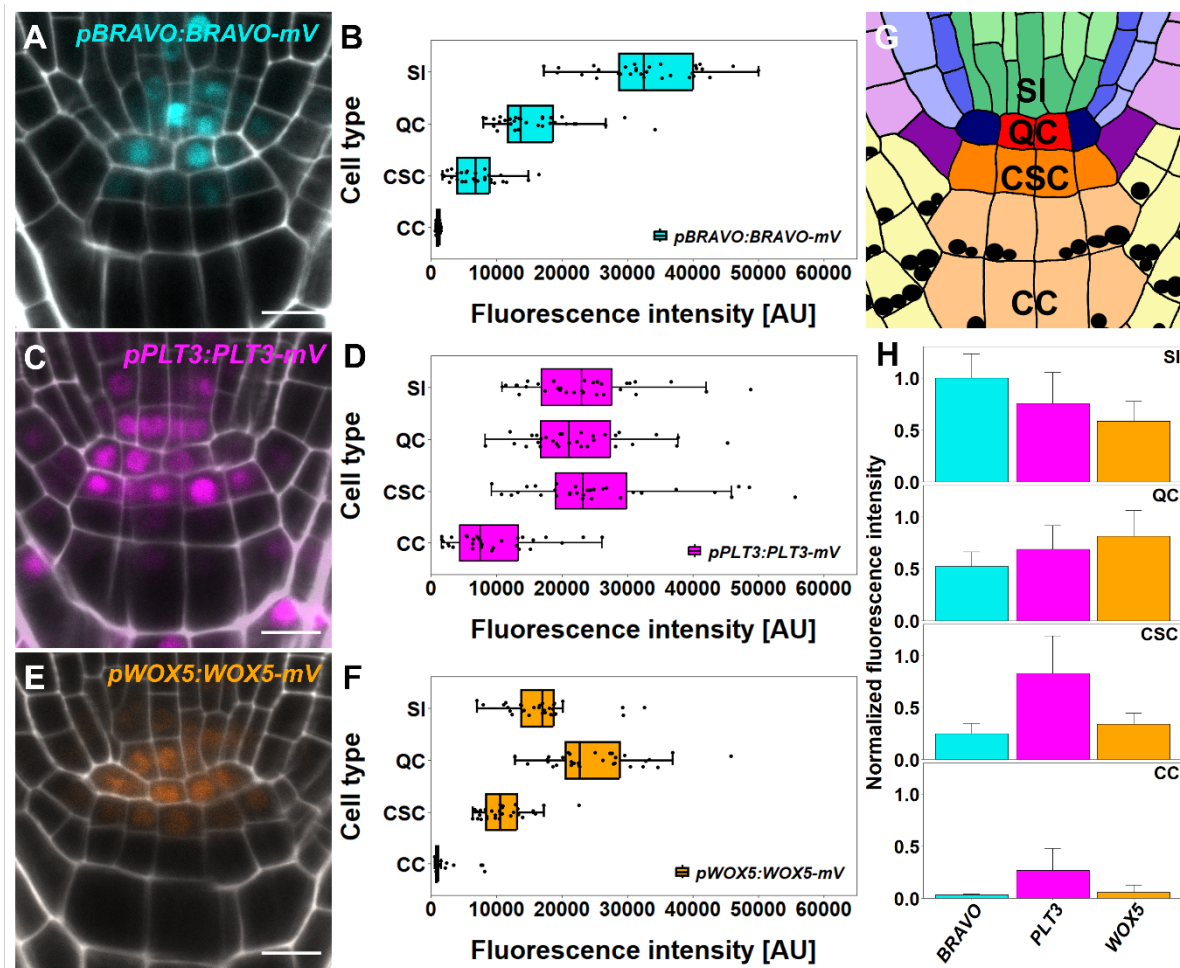
Figure 1: Abundance of BRAVO, PLT3 and WOX5 in the Arabidopsis RAM. Representative images of translational reporter of **A)** BRAVO, **C)** PLT3 and **E)** WOX5 in wildtype *Col-0* background in the RAM as well as the cell type specific quantification of mVenus (mV) fluorescence intensity in **B)** for BRAVO, **D)** for PLT3 and **F)** for WOX5. **G)** Schematic overview of the organisation of the Arabidopsis RAM. The different cell types are represented by different colours. QC: red, cortex endodermis initial: dark blue, endodermis: mid blue, cortex: light blue, stele initials (SI): green, stele: light green, lateral root cap/epidermis initial: purple, epidermis: light purple, lateral root cap: light yellow, columella stem cell (CSC): orange and columella cell (CC): light orange. Starch granules are visualised as black dots. **H)** Bar plot representing the mean fluorescence intensities of mV in BRAVO, PLT3 or WOX5 translational reporters in SIs, QCs, CSCs and CCs normalized to the maximum intensity found for BRAVO in SIs. Error bars display standard deviation. Cell walls were stained using PI and are shown in white, expression of TF is visualized by mVenus in cyan (BRAVO), pink (PLT3) or orange (WOX5). Scalebars represent 10 μm.
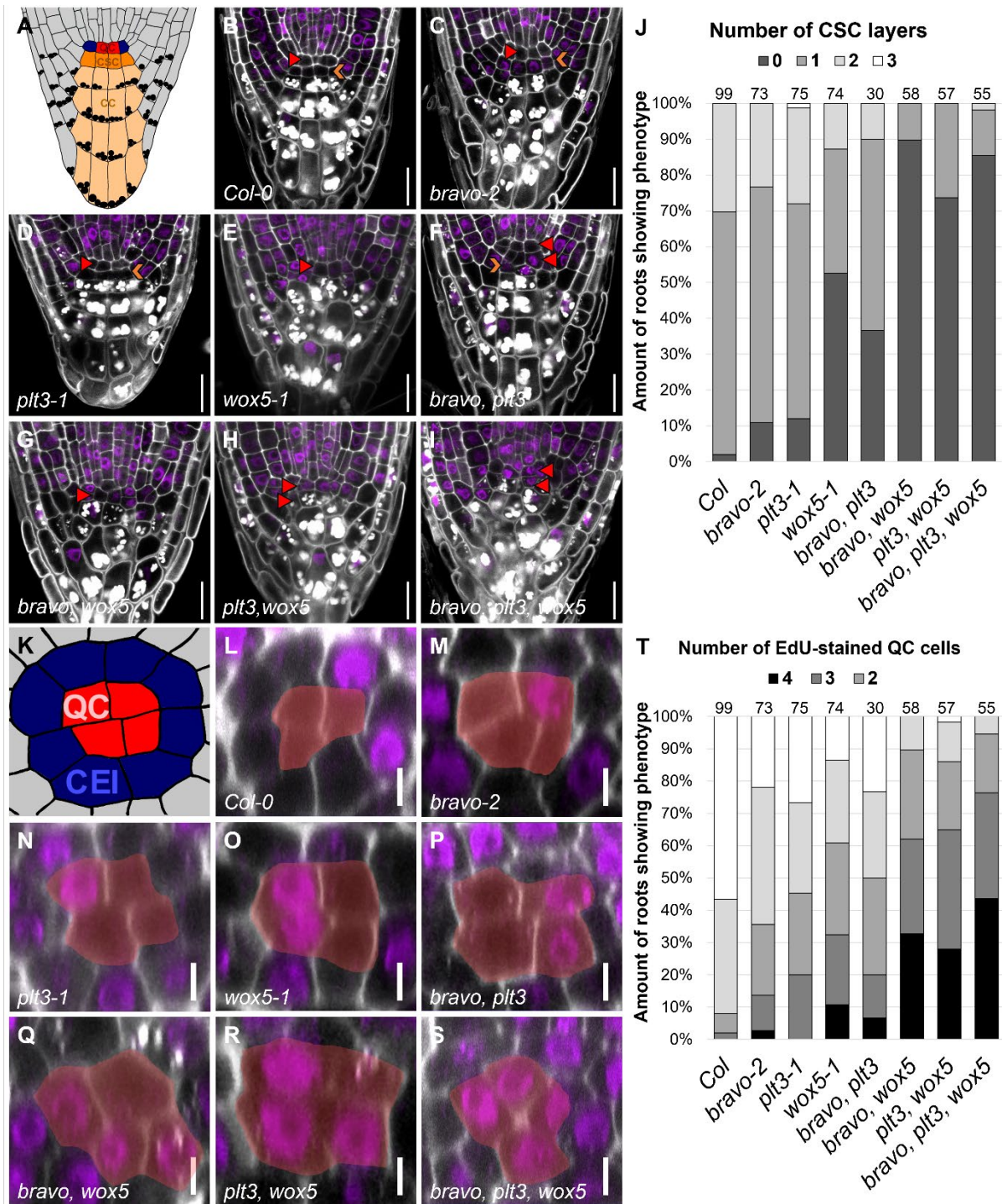
Figure 2: BRAVO, PLT3 and WOX5 jointly regulate CSC differentiation and QC quiescence. A) Schematic representation of a longitudinal section of the Arabidopsis RAM. Red: QC, blue: CEI, dark orange: CSC, light orange: CC. **B-I)** Representative images of the mutant CSC phenotype in the indicated mutant background after combined mPSPI (white) EdU (purple) staining. The position of the QC is indicated by a red arrowhead and the CSC layer is marked with an orange arrowhead. Scale bars represent 20 μm. **J)** Quantification of SCN staining displaying 0, 1, 2 or 3 layers of CSC. The number of analyzed roots for each genotype is

37

1114   indicated above each bar and results from to 3-5 technical replicates. **K)** Schematic

1115   representation of a transversal section of the Arabidopsis RAM. QC cells are

1116   highlighted in red and CEIs are displayed in blue. **L-S)** Representative images of

1117   optical cross sections of the Arabidopsis RAM in the indicated mutant background.

1118   The combined mPSPI/EdU staining reveals the cells that have divided within 24 h.

1119   QC is highlighted in yellow. Scale bars represent 5 µm **T)** Quantification of SCN

1120   staining displaying 0, 1, 2, 3 or 4 or more QC divisions. The number of analyzed

1121   roots for each genotype is indicated above each bar and result from to 3-5 technical

1122   replicates.
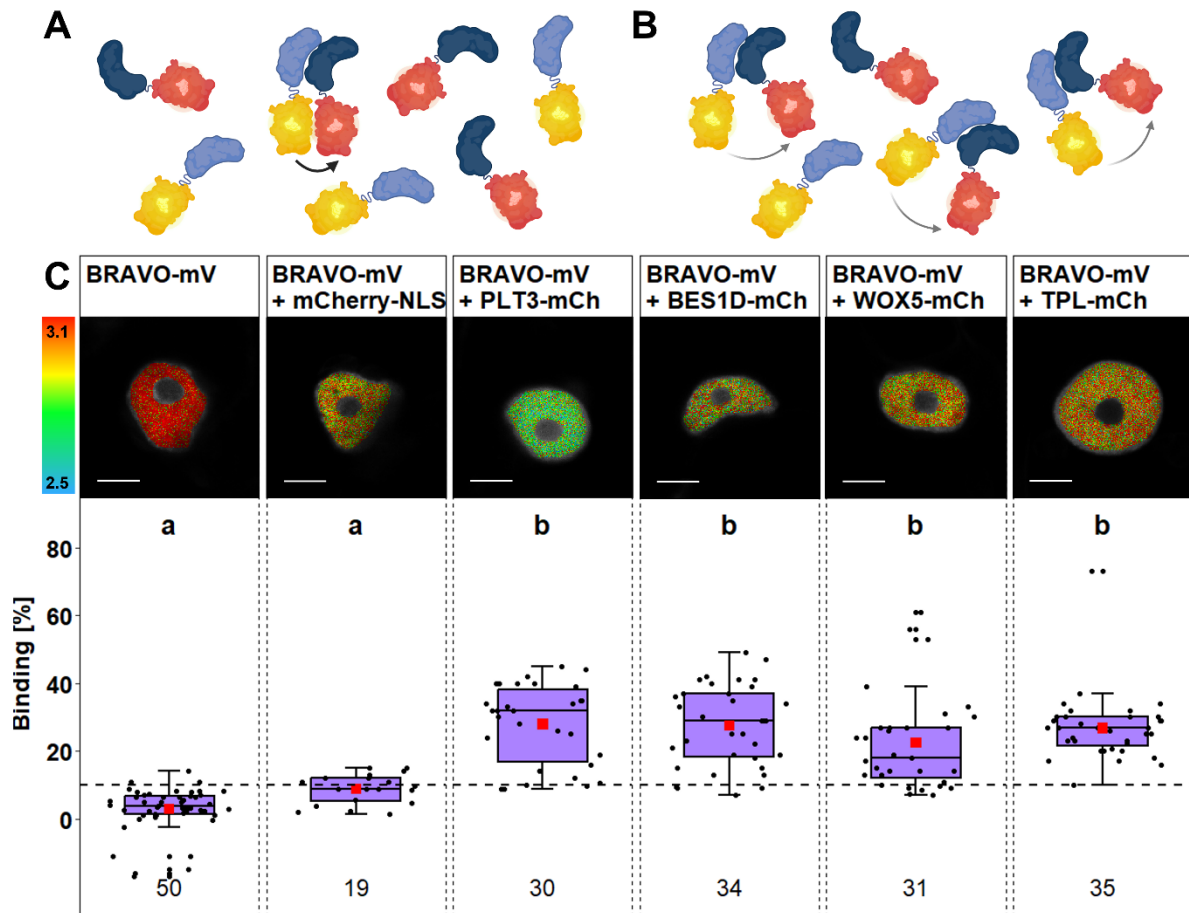
Figure 3: BRAVO interacts with PLT3, WOX5, BES1D and TPL. A) A reduction of fluorescence lifetime as a consequence of FRET can either be a result of a highly efficient energy transfer indicating close proximity or **B)** a high affinity of the two proteins. Figure created with BioRender.com and modified from (Maika *et al.*, 2023). **C) Upper panel:** Representative images of fluorescence lifetime imaging microscopy (FLIM) measurements of nuclei in *N. benthamiana* epidermal leaf cells after pixel-wise mono- or biexponential fitting. The fluorescence lifetime of the donor BRAVO-mV in absence or presence of the indicated acceptor (of mCherry-NLS, PLT3-mCh, BES1D-mCh, WOX5-mCh or TPL-mCh) is color-coded: blue (2.5) refers to low fluorescence lifetime [in ns], red (3.1) indicates high fluorescence lifetime [in ns]. Scale bars represent 6 μm. **Lower panel:** Binding values [%] are represented as purple box plots of the same samples as in the upper panel. Statistical groups were assigned after a non-parametric Kruskal-Wallis ANOVA with *post-hoc* Dunn's test ($\alpha = 0.05$). Mean values are visualised as red squares. Black dotted line indicates the Binding cut-off of 10 %. Number of analysed nuclei is indicated below each sample and results from 3-5 technical replicates. Partially created with BioRender.com.
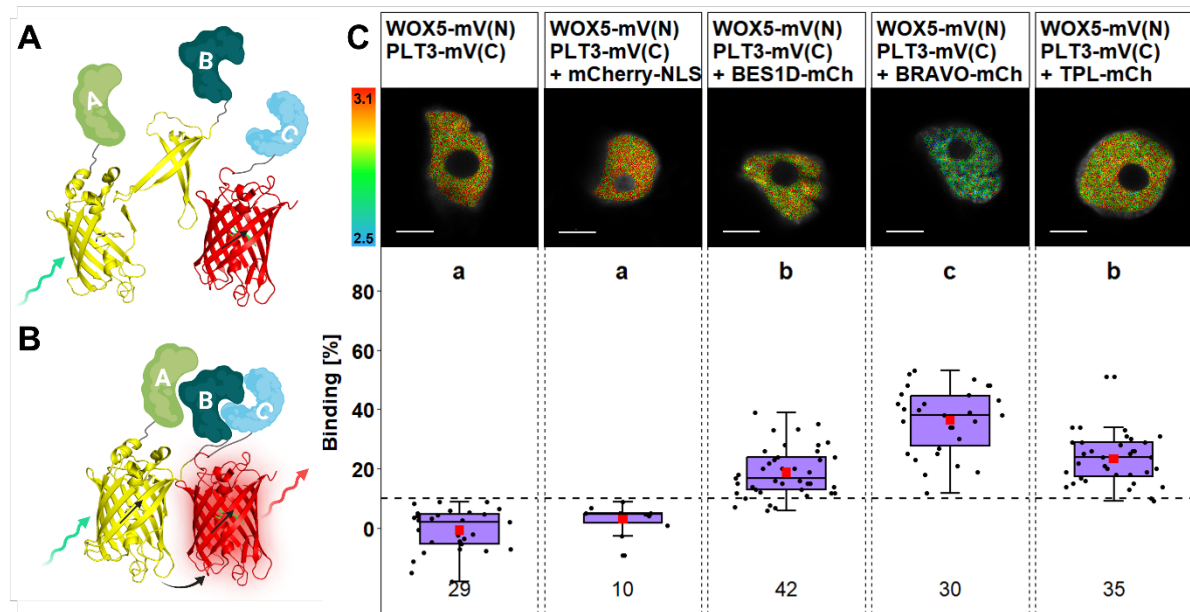
39

Figure 4: Trimeric complex formation of WOX5 and PLT3 with BRAVO, BES1D and TPL. A) The combination of BiFC-FRET allows the detection of higher-order complexes. Here, the two fragments of a split donor fluorophore are fused to two proteins of interest (POI), while a third POI is fused to the acceptor. **B)** In case of trimeric complex formation, the donor molecule is reconstructed and transfer energy to the acceptor molecule by FRET after excitation. Created with BioRender.com and modified from (Strotmann and Stahl, 2022). **C) Upper panel:** Representative images of fluorescence lifetime imaging microscopy (FLIM) measurements of nuclei *N. benthamiana* epidermal leaf cells after pixel-wise mono- or biexponential fitting. The fluorescence lifetime of the donor WOX5-mV(N)/PLT3-mV(C) in absence or presence of the indicated acceptor (mCherry-NLS, BES1D-mCh, BRAVO-mCh or TPL-mCh) is color-coded: blue (2.5) refers to low fluorescence lifetime [in ns], red (3.1) indicates high fluorescence lifetime. Scale bars represent 6 μm. **Lower panel:** Binding values [%] are represented as purple boxplots of the same samples as in the upper panel. Statistical groups were assigned after non-parametric Kruskal Wallis ANOVA with *post-hoc* Dunn's test (α = 0.05). Mean values are visualised as red squares. Black dotted line indicates the Binding cut-off of 10 %. Number of analysed nuclei is indicated below each sample and results from 2-3 technical replicates. Partially created with BioRender.com.

40
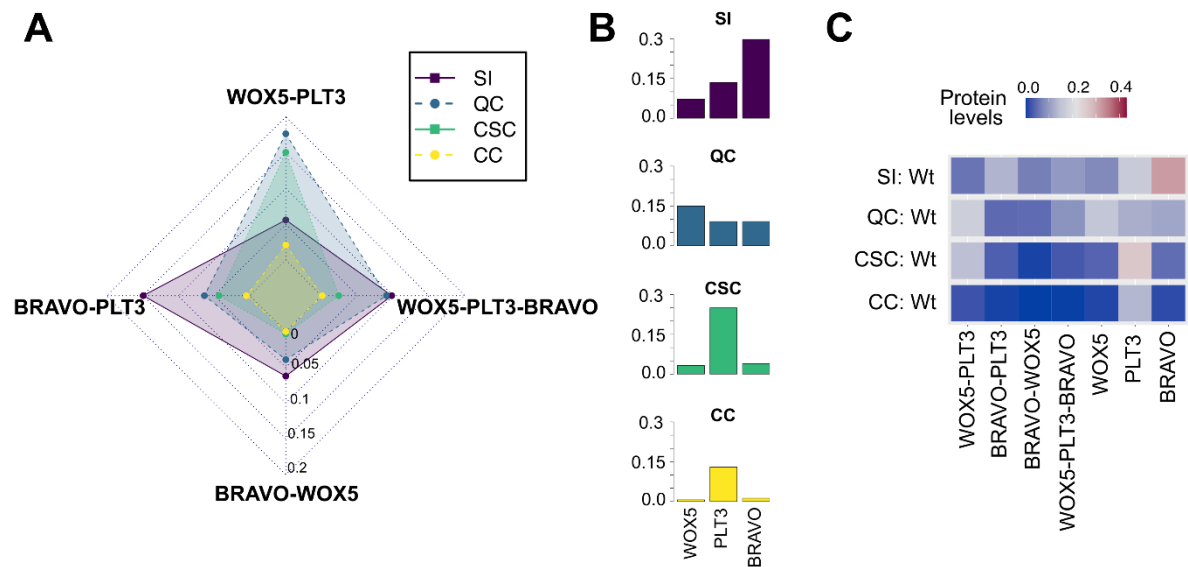
Figure 5. *In silico* prediction of protein complex signatures in the WT root SCN.
A) Radar plot showing the levels of heterodimers and trimeric complex of WOX5, PLT3 and BRAVO formed in the SI (purple), QC (blue), CSC (green) and CC (yellow). The radial axis shows the protein levels (in arbitrary units). **B)** Free WOX5, PLT3 and BRAVO protein in each of the simulated root SCN cells. **C)** Heatmap showing the protein complexes and free protein in the cells of WT simulation. High concentrations are displayed in red, low concentration are displayed in blue. SI: stele initals; QC: quiescent center; CSC: columella stem cells; CC: columella cells.
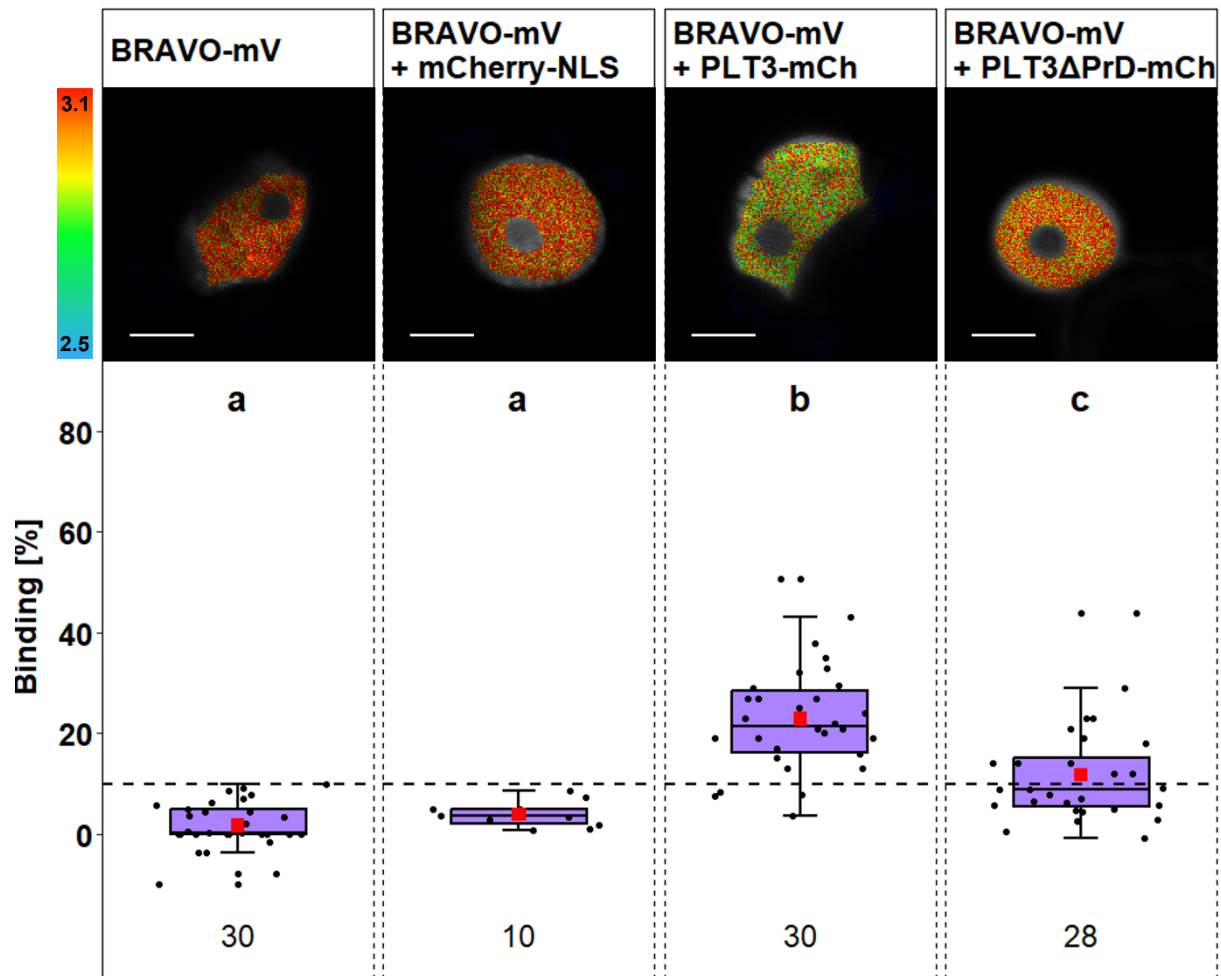
41

Figure 6: PrDs of PLT3 stabilize interaction with BRAVO. Upper panel: Representative images of fluorescence lifetime imaging microscopy (FLIM) measurements of nuclei in *N. benthamiana* epidermal leaf cells after pixel-wise mono- or biexponential fitting. The fluorescence lifetime of the donor BRAVO-mV in absence or presence of the indicated acceptor (mCherry-NLS, PLT3-mCh or PLT3dPrD-mCh) is color-coded: blue (2.5) refers to low fluorescence lifetime [in ns], red (3.1) indicates high fluorescence lifetime. Scale bars represent 6 µm. **Lower panel:** Binding values [%] are displayed as purple box plots of the same samples as the upper panel. Statistical groups were assigned after non-parametric Kruskal Wallis ANOVA with *post-hoc* Dunn's test ($\alpha = 0.05$). Mean values are visualised as red squares. Black dotted line indicates the Binding cut-off of 10 %. Number of analysed nuclei is indicated below each sample and results from 2-3 technical replicates.

42
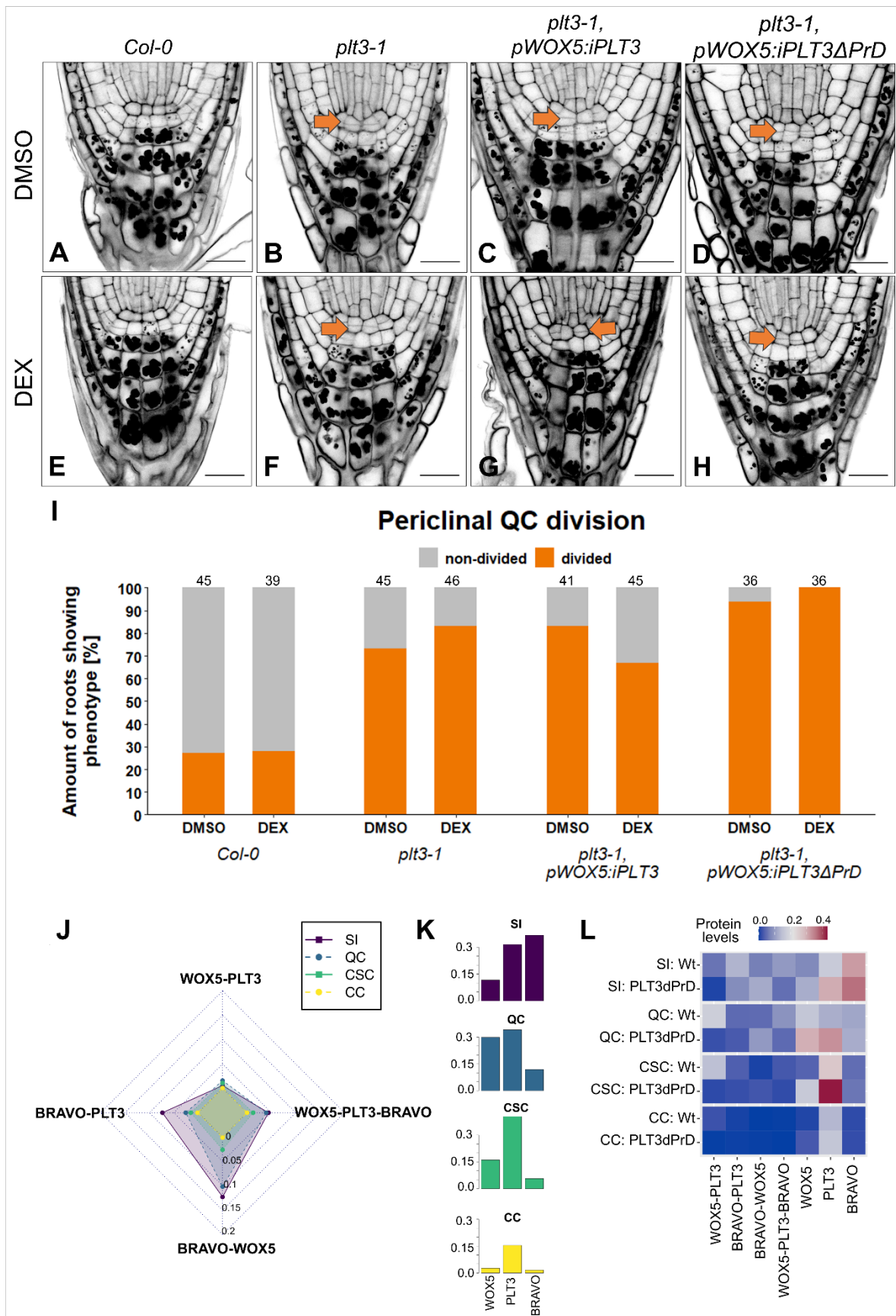
1184

Figure 7. PLT3 PrDs inhibit periclinal QC divisions and *in silico* predicted protein complex signatures in the root SCN. Representative images of the

1187 *Arabidopsis* root meristem showing additional periclinal cell divisions in the QC in

1188 the absence **A-D)** or presence **E-H)** of DEX in the indicated genetic background.

1189 Divided QCs are highlighted with orange arrows. Scalebars represent 20 μm. **I)**

1190 Quantification of periclinal cell divisions when roots are treated with DMSO or DEX.

1191 Number of analysed roots is indicated above each bar and results from three

1192 replicates. **J)** Radar plot showing the levels of heterodimers and trimeric complex

1193 between WOX5, PLT3 and BRAVO formed in the stele initials (purple), QC (blue),

1194 CSC (green) and CC (yellow). **K)** Free WOX5, PLT3 and BRAVO protein in each of

1195 the simulated root SCN cells. **L)** Heatmap showing the protein complexes and free

1196 protein in the cells of WT and PLT3ΔPrD simulations, the profiles are visibly different

1197 with a marked increase in free PLT3 in the CSC. High concentrations are displayed

1198 in red, low concentration are displayed in blue. SI: stele initials; QC: quiescent

1199 center; CSC: columella stem cells; CC: columella cells.
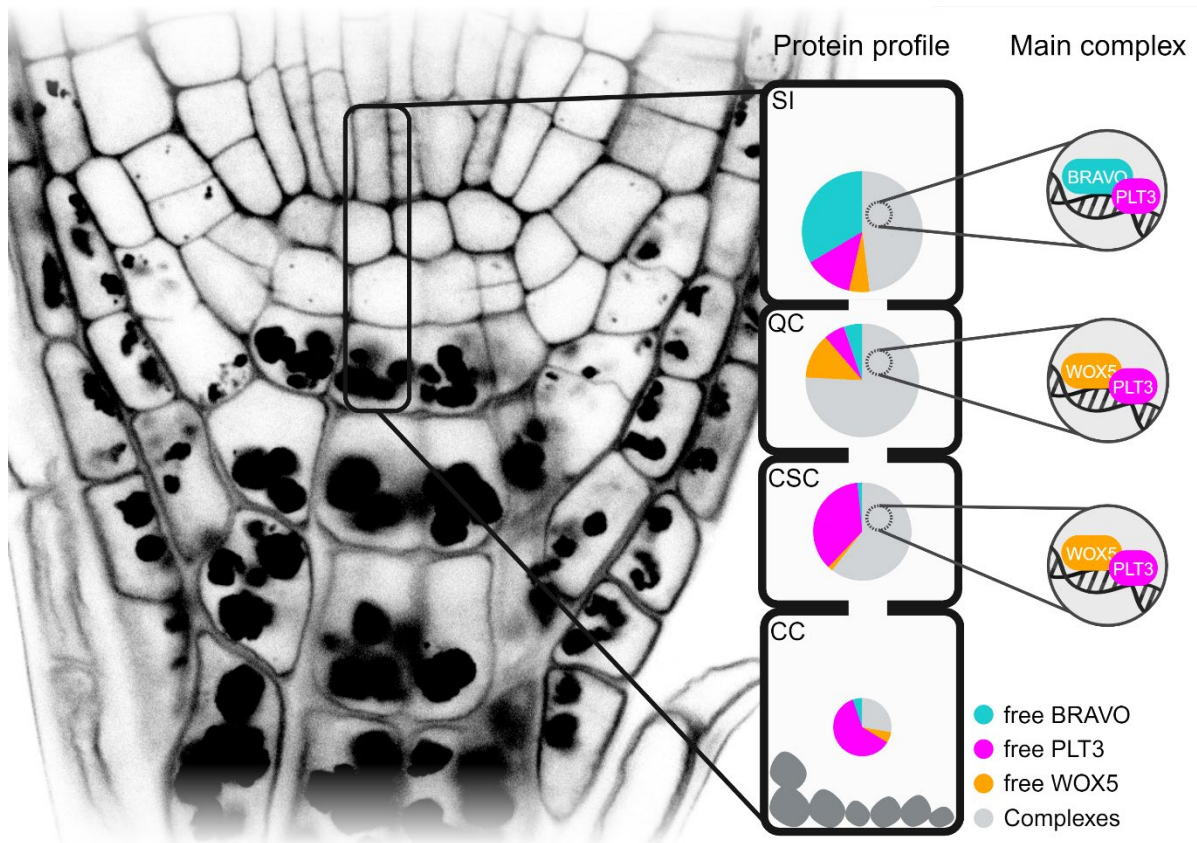
Figure 8: Model of protein signatures and complexes in the root SCN. The nuclei of different cell types (SI, QC, CSC, CC) show distinct protein profile of free BRAVO (turquoise), PLT3 (magenta), and WOX5 (orange) protein levels and main complexes (gray and insets). The size of the pie chart reflects the overall protein concentration in the nuclei of the specific cell type from high concentration (big) to low concentration (small). Created with BioRender.com.